UNIVERSITÀ
DEGLI STUDI
DI PADOVA

DIPARTIMENTO
DI INGEGNERIA
DELL'INFORMAZIONE

DIPARTIMENTO DI INGEGNERIA DELL'INFORMAZIONE

CORSO DI LAUREA IN BIOINGEGNERIA PER LE NEUROSCIENZA

Analysis of the blood-to-brain tracer exchange in [^{18}F] DPA714 PET imaging

Relatore: Prof. Mattia Veronese

Laureanda: MICHELLE CARRANZA MELLANA

Correlatori: Lucia Maccioni, Benedetta Bodini

ANNO ACCADEMICO 2022-2023

Data di laurea 09/10/2023

INDEX

ABSTRACT [Eng]

Neuroinflammation has a pivotal role in chronic neurodegenerative conditions, including multiple sclerosis (MS). Microglial cell activation is a key feature of neuroinflammation, and TSPO PET imaging plays a centra role in quantifying activated microglia in vivo.

The widely used 2T4K kinetic model facilitates the quantification of TSPO PET tracers, with the influx rate constant K_1 emerging as a promising biomarker linked to blood-brain barrier permeability and cerebral blood flow. The study highlights recent findings suggesting K_1 as a biomarker for changes in blood-brain barrier permeability due to peripheral inflammation. Addressing the drawback of invasive blood sampling, the study introduces a novel approach — 1T1K-IDIF, a blood-free method for estimating K_1. The study presents evidence supporting the viability of this method as an alternative for assessing blood-to-brain tracer exchange in TSPO PET studies.

Initial validation with subjects having arterial input functions correlates K1 values from the full compartmental model with those from the reduced compartmental model. Sensitivity analysis and test-retest assessments were made. The impact of physiological factors on K1 estimates through a linear mixed-effects model and stepwise regression was also examined.

In the context of MS progression and treatment assessment, the thesis aims to analyse brain-to-blood exchanges in [18F] DPA714 PET imaging within the grey matter cortex, white matter lesions, and normal-appearing white matter. Comparisons with healthy subjects and intra-patient comparisons between NAWM, lesions, and GM cortex provide insights into BBB transfer rates in MS.

ABSTRACT [Ita]

La neuroinfiammazione gioca un ruolo cruciale nelle condizioni neurodegenerative croniche, annoverando anche la sclerosi multipla (SM).

L'attivazione delle cellule microgliali è una caratteristica chiave della disciplina in esame e l'imaging TSPO PET è determinate nella quantificazione delle microglie attivate in vivo. Il modello cinetico 2T4K, ampiamente utilizzato, facilita la quantificazione dei traccianti PET di TSPO, con la costante di velocità di ingresso K_1. Questa costante emerge come un promettente biomarcatore ed è legato alla permeabilità della barriera emato-encefalica e al flusso sanguigno cerebrale. Affrontando l'inconveniente del prelievo invasivo di sangue, lo studio introduce un approccio innovativo, il 1T1K-IDIF, un metodo che non prevede il prelievo di sangue arterioso per stimare il K_1. L'indagine presenta prove a sostegno della validità di questo metodo come alternativa per valutare lo scambio di traccianti dal sangue al cervello negli studi PET di TSPO.

La validazione iniziale, eseguita con soggetti che hanno la funzione di input arterioso, correla i valori di K_1 del modello compartimentale completo, con quelli del modello compartimentale ridotto. Inoltre, sono state effettuate analisi di sensibilità e valutazioni di riproducibilità; è stato valutato l'impatto dei fattori fisiologici nelle stime di K_1attraverso un modello lineare a effetti misti e una regressione stepwise.

Nel contesto della progressione e della valutazione del trattamento della sclerosi multipla (SM), la tesi mira ad analizzare gli scambi sangue-cervello nell'immagine PET di [^{18}F] DPA714 nella corteccia della materia grigia, nelle lesioni della materia bianca e nella materia bianca di aspetto normale. Il confronto dei valori di K1 della corteccia con quelli dei soggetti sani e i confronti intra-paziente tra la materia bianca dall'aspetto normale e le lesioni della materia grigia forniscono informazioni sui tassi di trasferimento della barriera emato-encefalica nella SM.

FOREWORD

Neuroinflammation is widely recognized as a pivotal factor in the onset and progression of chronic neurodegenerative conditions, including multiple sclerosis (MS), which we will focus on, Alzheimer's disease (AD), and Parkinson's disease (PD). This inflammatory process is notably characterized by the activation of microglial cells, which are central to the neuroinflammatory response in these disorders (Glass et al., 2010). Given the importance of identifying potential targets for anti-inflammatory neuroprotective interventions, the availability of a reliable imaging tool capable of quantifying activated microglia in real-time holds immense promise (Bodini et al., 2021).

The research on neuroinflammation has been significantly impacted by TSPO Positron Emission Tomography (PET) imaging, which holds a key role in this field. PET is a powerful resource for the in vivo study of neuroinflammatory processes (Jain et al., 2020; Turkheimer et al., 2015; Werry et al., 2019), that exploits radiotracers specifically binding the translocator protein 18 kDa (TSPO), formerly known as the peripheral benzodiazepine receptor. TSPO is generally assumed to be a biomarker of neuroinflammation that is substantially upregulated in activated microglia in neuro-immune responses (Jain et al., 2020). While it remains minimally expressed in the quiescent brain by resting microglial cells, its expression markedly surges upon microglial activation (Vennetti et al., 2013). This phenomenon positions TSPO as a valuable imaging target, offering the potential to visualize and quantify the activation status of microglia in vivo.

The quantification of dynamic PET imaging requires compartmental modeling, which gives a mathematical explanation of the kinetics of radiotracer movement inside the target tissues as a function of the tracer concentration in the plasma (C_p). While the model parameters characterize the tracer kinetics, C_p often determines the input function of the model. The most used kinetic model for TSPO PET tracers is 2T4K, which has two reversible compartments and four rate constants (i.e., K_1, k_2, k_3, k_4) (Turkheimer et al., 2015; Wimberley et al., 2021). Among the microparameters, the influx rate constant K1 (ml/cm3/min), namely the rate at which the tracer from plasma or blood compartment crosses the blood-brain barrier (BBB), represents a promising biomarker for the detection of pathological processes in brain diseases due to its relation to the cerebral blood flow (F, ml/cm3/min) and the unidirectional extraction fraction from blood into the brain during the tracer's first pass through the capillary bed (E). Ultimately,

using the Fick principle and the Renkin-Crone model, K1 depends on perfusion and the product of capillary permeability P (cm/min) and capillary surface area S (cm2/cm3), P×S [Renkin, 1959; Crone, 1963]. Recent findings indicate that the rate of blood-to-brain influx (K1) could be a valuable biomarker of changes in blood-brain barrier permeability of TSPO radioligands linked to peripheral inflammation (Nettis et al., 2020; Turkheimer et al., 2015).

Nonetheless, the conventional approach of using compartmental modeling for quantification has a primary drawback: it necessitates invasive blood sampling and intricate protocols to establish the arterial input function. To address this limitation, a novel approach has been adopted in this study. A simplified blood-free methodologic framework has been employed for estimating K1. This involves fitting the early phase tracer dynamics using a single irreversible compartment model and an image derived input function (1T1K-IDIF). The evidence collected strongly supports the viability of the 1T1K-IDIF method as a blood-free alternative to assess blood to-brain tracer exchange in TSPO PET studies. Nonetheless, the conventional approach of using compartmental modeling for quantification has a primary drawback: it necessitates invasive blood sampling and intricate protocols to establish the arterial input function. To address this limitation, a novel approach has been adopted in this study. A simplified blood-free methodologic framework has been employed for estimating K1. This involves fitting the early phase tracer dynamics using a single irreversible compartment model and an image derived input function (1T1K-IDIF). The evidence collected strongly supports the viability of the 1T1K-IDIF method as a blood-free alternative to assess blood to-brain tracer exchange in TSPO PET studies.

In the context of multiple sclerosis (MS) progression and treatment assessment, a method that can accurately quantify subtle blood-brain barrier (BBB) disruption both within lesions and in non-lesional areas holds significant value. This approach could provide crucial insights into the disease's advancement and the effectiveness of interventions.

The primary goal of this study was to perform an analysis of the blood-brain barrier (BBB) tracer exchange, often denoted as K_1, in [^{18}F] DPA714 PET imaging within the grey matter cortex in a cohort of twenty-two patients with multiple sclerosis (MS) and seventy-nine healthy controls (HC).

In the initial phase of the study, a cohort of eight subjects with available arterial input functions was utilized to establish the validity of the bloodless technique. This validation was achieved

by correlating the K1 values derived from the full compartmental model with those obtained through the reduced compartmental model 1T1K-IDIF ($\rho = 0.93 \pm 0.05\%$). To ensure reliable K_1 estimation, a sensitivity analysis was performed to pinpoint the optimal time window within the early phase tracer dynamics. Subsequently, the study assessed repeatability using the mean relative difference (MRD) in a cohort of eight test-retest healthy volunteers. Following this, the impact of factors such as aging, gender, genotype, dose-to-weight ratio, and BMI on K1 values was investigated through the implementation of a linear mixed-effects model.

Using a consistent methodology, the blood-brain barrier (BBB) transfer rate (K_1) was measured in lesions in the white matter, normal-appearing white matter (NAMW), and grey matter (GM) cortex in individuals with multiple sclerosis. The quantified K_1 values of the GM cortex were compared to those obtained from the group of healthy subjects, and for each multiple sclerosis's patient, the normal appearing (NAWM) and lesions were also contrasted.

Chapter 1 -

MULTIPLE SCLEROSIS

Multiple sclerosis (MS) is an inflammatory disease of the central nervous system (CNS) with inflammatory and degenerative components affecting both the white (WM) and grey matter (GM). The fundamental pathological features of MS encompass inflammation with demyelination, failure of remyelination, astroglia proliferation (gliosis), and neurodegeneration, which affect the white matter and the grey matter both locally and diffusely (Hauser & Cree, 2020). Since the first characterization, the overall pathology of MS has been thoroughly defined (Haider et al., 2016; Lassmann, 2018).

In MS, auto-aggressive T-cells are believed to penetrate the blood-brain barrier (BBB), causing demyelination and axonal loss that eventually result in progressive neurological impairment. MS is primarily assumed to be an immune-mediated illness of the central nervous system (CNS). Extensive research has highlighted leukocyte transit through the BBB as being of utmost significance for disease pathogenesis (Ortiz et al., 2014). Histopathological studies have reported abnormalities of this barrier in inactive MS lesions as well as normal appearing white matter (Misra et al., 2003; Odoardi et al., 2012).

During the disease course, the interaction of inflammatory and neurodegenerative processes in MS often causes episodes of transient neurological dysfunction followed by progressively increasing impairment. Myelin is destroyed in the brain and spinal cord during an MS episode, which causes inflammation in certain CNS white matter regions and leads to progressive impairment over the course of the disease. Motor dysfunction, sensory disturbances, tremor, nystagmus, loss of coordination or balance, numbness, problems in speech and vision, and cognitive impairment are some of the clinical signs of MS (Ortiz et al., 2014).

Current therapies for MS are very effective in targeting the immune system and in preventing clinical relapses but fail to prevent or delay neuro-axonal degeneration and, as a result, clinical progression (Ontaneda et al., 2015). A cure that is able to stop the disability progression is still lacking, and the precise origins of the disease remain only partially understood.

1.1 Epidemiology

Multiple sclerosis (MS) constitutes a global challenge, with its prevalence exhibiting an upward trend. Globally, females are more likely to have MS than males (Trojano et al., 2017). MS primarily affects young adults, with onset between 20 and 40 years of age (Greer & McCombe, 2011). The neuro-axonal damage can even start during the preclinical stage of MS and progresses gradually before manifesting clinically as an accumulation of disability (Kawachi & Lassmann, 2017; McGinley & Ontaneda, 2019).

The estimated number of people with MS worldwide has increased to 2.8 million in 2020 (Walton et al., 2020), with a demographic and gender heterogeneity. The highest prevalence rates, exceeding 120 cases per 100,000 population, are observed in North America, and some northern European countries. Conversely, regions located around the equator witness lower prevalence rates, falling below 60 cases per 100,000 population. The latitudinal gradient may be explained by genetic reasons, but also environmental risk factors that change with latitude may also be involved. Genetic factors certainly play a role in the pathophysiology of MS, particularly the distribution of the HLA-DRB1 haplotype. Several decades ago, researchers discovered a link between MS and polymorphisms in the human leukocyte antigen (HLA) genes found in the major histocompatibility complex (Jersild et al., 1972). For instance, it has been demonstrated that individuals who carry the class II variation HLA DRB1*15:01 allele have a roughly threefold increased risk of developing the disease (Patsopoulos et al., 2013). Meanwhile, the most likely candidate among the environmental risks is the reduced levels of vitamin D, caused by a lack of sun exposure, and has been linked to an increased risk of multiple sclerosis (Ascherio et al., 2014). Other environmental risks have also been discovered, including Epstein-Barr virus infection (Bjornevik et al., 2022), cigarette smoking (Ramanujam et al., 2015), organic solvent, and adolescent obesity (Olsson et al., 2016). Nighttime employment, heavy alcohol or caffeine usage, and a history of infectious mononucleosis are other, less well-established risk factors (Olsson et al., 2016). In addition, air pollutants may be one of the possible environmental risk factors for MS (Tateo et al., 2019) as suggested by the work of Tateo and colleagues, who investigated the association of PM2.5 with MS prevalence in the North-East Italy, one of the most pollutes geographical areas of Italy. Although it is recognized that environmental risk factors and genetic predisposition interact to develop MS, its exact causes are still unknown.

1.2 Clinical subtypes of MS

The vast clinical variety of MS has traditionally been broken down into three primary categories: relapsing-remitting, secondary progressive, and primary progressive MS (Filippi et al., 2014; Thompson et al., 2018).

Relapsing-remitting MS (RRMS) is the most common form of the disease. It is typically characterized by episodic and reversible stages of neurological impairments lasting at least 24 hours and up to several weeks, the so-called relapses. Secondary progressive MS (SPMS) develops over the course of RRMS and with repeated relapses in the absence of therapeutic intervention, progresses to persistent neurological impairments and disability over a median period of 20 years (range 1-51 years) (Cree et al., 2021). Primary progressive MS (PPMS) has a more insidious progressive course with gradually worsening neurological dysfunction from onset. It affects a small percentage of people (about 10-15 %) (Lublin et al., 2014), who are often older men at illness onset (Miller & Leary, 2007).

Finally, the disease can be further characterized as active or non-active within each subgroup by the presence of clinical or neuroimaging activity, which is determined by clinical relapses and/or MRI activity (contrast-enhancing lesions; new or unequivocally enlarging T2 lesions assessed at least annually) (Lublin et al., 2014). Additionally, people with PPMS or SPMS can be categorized based on whether their disability has worsened over time (Krieger et al., 2016; Lublin et al., 2014).

Finally, growing body of research indicates that neurodegeneration plays a crucial role in the pathogenesis of MS throughout the course of the disease, including not only the progressive forms of MS, but also the relapsing-remitting form (Bodini et al., 2021).

1.3 Mechanisms/pathophysiology

According to conventional wisdom, multiple sclerosis is a chronic inflammatory-demyelinating illness of the central nervous system (CNS) that causes the development of demyelinated plaques with varying degrees of axonal preservation and reactive astrocytic scar formation. Beginning with the macroscopic illustrations of changes to the brain and spinal cord by (Carswell, 1833), several fundamental MS pathology characteristics were described during the 19th century (Cruveilhier J, 1833). Following these findings, Charcot was the first to accurately

identify MS's primary pathology characteristics and describe the condition as a focal inflammatory demyelinating illness of the white matter (Charcot JM, 1868).

For a while, it was believed that MS was a neurological condition caused solely by white matter focal demyelinated plaques. Later, it was discovered that demyelinated lesions can be seen not only in the WM, due to the abundance of myelin, but also in the grey matter (GM) (Kutzelnigg et al., 2005; Peterson et al., 2001), which includes the cortex, and the deep GM. Evidence suggests that cortical lesions are a major cause of clinical disability, especially in patients with progressive MS (Calabrese et al., 2012; Magliozzi, Reynolds, et al., 2018). Furthermore, regardless of the clinical manifestations of the disease, a gradual process of neurodegeneration that damages the brain and spinal cord has been demonstrated to emerge since the earliest stages of the disease course (Borgström et al., 2020; Lazzarotto et al., 2020; Margoni et al., 2021).

The idea of a disrupted BBB as a prerequisite for developing MS is not new. Poser in 1986 (Dodelet-Devillers et al., 2009) proposed a theory in which four states that four factors must occur for MS to manifest: genetic susceptibility; an environmental event that is likely immune-mediated by a virus; an alteration in BBB function; and the formation of myelinoclastic plaques in the central nervous system (Cramer et al., 2014; Münzel & Williams, 2013). Focal plaques (also known as lesions), that are regions of demyelination, typically located around post capillary venules and characterized by disruption of the BBB, are the pathological hallmark of all multiple sclerosis phenotypes. Although the exact mechanisms of BBB disintegration are not well known, they appear to entail both direct and indirect effects of pro-inflammatory cytokines and chemokines (such as TNF, IL1 and IL 6) produced by resident cells and endothelial cells (Minagar & Alexander, 2003; Ortiz et al., 2014). When the BBB is dysregulated, more activated leukocytes, such as macrophages, T cells, and B cells, migrate across the endothelium and into the central nervous system (CNS). This causes more inflammation and demyelination, which is followed by oligodendrocyte loss, reactive gliosis, and neuronal axonal degeneration (Frohman et al., 2006; C. Lucchinetti et al., 2000). Although recurrence may be seen in the same or other areas within an interval of weeks, months, or even years, the breakdown of the BBB in MS is assumed to be transitory. Axonal transection to varying degrees, new phases of BBB leaking, and immunologically induced demyelination are all parts of the subsequent development and progression of the lesions. It is well known that neuroinflammatory and infectious events alter the expression and structure of junctional proteins (Cassan & Liblau, 2007; Nair et al., 2008).

Plaques are common throughout the CNS, particularly in the brain, optic nerve, and spinal cord, and can arise in both white matter and grey matter (Gilmore et al., 2009; Petrova et al., 2018). The total volume of these lesions is only moderately correlated with overall clinical disability and cognitive impairment despite the anatomical location of white matter lesions being associated with specific clinical manifestations of MS (Rocca et al., 2015; Sormani et al., 2009). This is due to the involvement of other pathophysiological mechanisms, such as the occurrence of grey matter lesions and normal-appearing brain tissue damage, which affect both grey matter and white matter.

1.3.1 White matter and grey matter lesions

Inflammation is a characteristic feature observed in and around multiple sclerosis (MS) lesions throughout all stages of the disease (Lassmann, 2018). While it is most prominent within actively demyelinating lesions, it is also present in inactive or remyelinated plaques, as well as in the normal-appearing white matter (Frischer et al., 2009).

Active demyelinating lesions are frequently present in the early stages of MS. Large, reactive (and occasionally multinucleated) astrocytes, activated microglia (especially at the lesion edge and containing myelin debris), macrophages (containing myelin debris), and significant lymphocyte infiltration (mainly $CD8^+$ T cells and $CD20^+$ B cells, with fewer $CD4^+$ T cells) are seen in these lesions (Frischer et al., 2015; Machado-Santos et al., 2018).

In contrast, due to a decrease in the frequency of inflammatory episodes in individuals with PPMS and SPMS, active demyelinating plaques are less common in these patients. Inactive lesions are the primary characteristic of PPMS and SPMS. In contrast to active lesions, inactive lesions are more clearly outlined, hypocellular, and have well-defined demyelination. They also have reduced axonal density, reactive astrocyte gliosis, variable microglial activation only in the periplaque white matter (without macrophages), and a lower lymphocyte density (Frischer et al., 2015; Prineas et al., 2001). In fact, active or mixed (inactive and active) lesions represented up to 57% of all lesions in patients with progressive MS in one investigation, and active lesions correlated with a more severe disease course (Luchetti et al., 2018). Nevertheless, inflammatory processes still play a role in PPMS and SPMS (Dendrou et al., 2015; Lassmann et al., 2012; Luchetti et al., 2018; Mahad et al., 2015).

Chronic active plaques and slow-expanding lesions are other types of plaques. A longer duration of the disease and SPMS patients are more likely to have chronic active plaques, which are characterized by macrophages at the lesion's perimeter and less macrophages in the lesion's centre. Slow expanding lesions, which are typically found in patients with SPMS, are characterized by an inactive centre with demyelination, activated microglia at the lesion edge and few macrophages containing myelin debris, but transected axons are also observed, suggesting a very slow rate of ongoing demyelination and axonal damage (Lassmann et al., 2012; Prineas et al., 2001; Rocca et al., 2015).

In MS patients, extensive cortical demyelination is seen in the forebrain (Klaver et al., 2013; Kutzelnigg et al., 2005), and cerebellum (Kutzelnigg et al., 2007), and it can be seen as early as the first stages of the disease. It is more common in patients with PPMS and SPMS, where >60% of the cortex can be affected in severe cases. Deep grey matter nuclei (Haider et al., 2014; Vercellino et al., 2009), and the spinal cord grey matter, which has more widespread and extensive grey matter demyelination than the white matter (Gilmore et al., 2009; Petrova et al., 2018), are further areas in which lesions can develop. Cortical lesions are frequently topographically associated to inflammatory infiltrates in the meninges and are predominately observed in cortical sulci and deep invaginations of the brain surface (Choi et al., 2012; Howell et al., 2011). Additionally, neuro axonal injury and widespread inflammation are present (Kutzelnigg et al., 2005; Mahad et al., 2015). Additionally, pro-inflammatory mediators released from the meninges or found in the cerebrospinal fluid are thought to facilitate their development (Magliozzi, Howell, et al., 2018). Cortical lesions typically exhibit less BBB breakdown, less oedema, a lower level of inflammation (characterized by fewer infiltrating activated microglia and macrophages (Peterson et al., 2001), and the remyelination is more extensive in the cortex compared with the white matter (Albert et al., 2007).This suggests that different mechanisms determine lesion formation in the white matter and the grey matter (Albert et al., 2007; Strijbis et al., 2017).

The long-term prognosis of deteriorating disability and cognitive impairment is supported by the assessment of cortical lesions and grey matter atrophy (M. Filippi et al., 2013; Rocca et al., 2017). Evaluation of grey matter damage may also be helpful for determining how well certain treatments work (Filippi et al., 2014).

The prevalence of cortical lesions, particularly band-like subpial lesions spreading over several adjacent gyri and sulci, is another defining aspect of progressive multiple sclerosis. T-cell and

B-cell infiltrates are uncommon within active cortical lesions in progressive multiple sclerosis in contrast to cortical lesions in acute and early multiple sclerosis, but continuous demyelinating activity is connected to meningeal inflammation (Magliozzi et al., 2007). At locations where microglia are activated, the cortex experiences active demyelination. Each patient has a different level of cortical demyelination. It typically affects between 20 and 30% of the cortex (Kutzelnigg et al., 2005), but in severe cases, it can affect up to 90 percent. A "cortico-spinal" type of multiple sclerosis, where significant cortical demyelination is present in the brain with no or few small focal white matter plaques, may result from subpial cortical demyelination that develops independently from white matter lesions (Trapp et al., 2018).

1.3.2 Normal appearing tissues

Normal appearing white matter (NAWM), frequently exhibits symptoms of diffuse inflammation and neuro axonal damage in addition to the localized lesions typically seen in MS patients (Kutzelnigg et al., 2005; Mahad et al., 2015).

Patients with progressive disease are more likely to experience severe NAWM abnormalities even if can be already observed in RRMS patients. Abnormalities of the NAWM include decreased fibre density caused by axonal degeneration and demyelination, small round cell infiltration (primarily lymphocytes), macrophage infiltration, widespread microglia activation, and gliosis (Kutzelnigg et al., 2005). NAWM was traditionally thought to be subsequent to the axonal damage within focal lesions, but these diffuse changes have a poor correlation with the number, size, location, and destructiveness of focal white matter lesions in the brain (Kutzelnigg et al., 2005) and spinal cord, suggesting that they may occur independently (Klaver et al., 2013).

Despite the challenging technical demands for conducting a reliable pathological and imaging investigation of normal-appearing white matter (NAWM) and normal-appearing grey matter (NAGM), it is evident that these regions exhibit significant pathological abnormalities. Consequently, these abnormalities hold the potential to elucidate the mechanisms behind clinical dysfunction, which may not be well-represented by macroscopically visible lesions (Miller et al., 2003).

1.4 Blood-brain barriers in MS

The disease is characterized by active inflammatory demyelinating lesions that develop with new waves of T and B lymphocytes that enter the central nervous system (CNS) in conjunction

with profound blood-brain barrier leakage at the early stages of the disease, as seen in patients with fulminant acute multiple sclerosis or in brain biopsies taken for diagnostic purposes (Frischer et al., 2015; Luchetti et al., 2018). Usually, gadolinium-contrast enhancement in MRI is used to show these lesions (Frank et al., 1994; Gaitán et al., 2011). The white matter is where these new active lesions are most frequently detected, although they can also be found in the deep grey matter nuclei or cerebral cortex with a lower incidence (Bevan et al., 2018; Kutzelnigg et al., 2005; C. F. Lucchinetti et al., 2011). Active lesions can be distinguished from inactive lesions by administering gadolinium-based contrast agents and acquiring post-contrast T1-weighted images; signal enhancement, which underlies active lesions, occurs as a result of increased BBB permeability and corresponds to regions with ongoing inflammation (Filippi et al., 2018).

Lastly, people with progressive illness have substantial widespread damage and atrophy of the normal-appearing white and grey matter in their brains. The secondary Wallerian degeneration brought on by axonal and neuronal injury in localized white and grey matter lesions is a contributing factor in the diffuse white matter damage (Absinta et al., 2020). Additionally, neuronal loss happens in lesions of the cortex as well as in the normal appearing cortex (Magliozzi et al., 2010) and seems to contribute more to widespread white matter degeneration compared with white matter lesions (Kutzelnigg et al., 2005). However, mechanisms other than those that cause axonal and neuronal damage in localized lesions, like meningeal inflammation, may also be a factor in the development of widespread white matter injury (Androdias et al., 2010; Haider et al., 2016). Clinical progression in multiple sclerosis is likely related to the accumulation of neuro-axonal loss in a lifelong inflammatory CNS environment (both adaptive and innate) and relative unbalance between damage, repair and brain functional reserve. Although the inflammatory process in progressive multiple sclerosis is not associated with overt blood-brain barrier damage, there is a moderate permeability increase in chronic active (Lee et al., 2018) as well as inactive lesions and this leads to a perivascular accumulation of fibrin (Yates et al., 2017). Fibrinogen deposition may contribute to progressive neurodegeneration as it may further activate microglia, induce demyelination, neurodegeneration and impair remyelination (Petersen et al., 2017; Trojano et al., 2017).

Demyelination and the development of lesions are closely linked to the breakdown of the blood-brain barrier (BBB), particularly in the vicinity of post-capillary venules, which are common locations for multiple sclerosis (MS) lesions (Filippi et al., 2019). This compromised BBB

permeability results in the infiltration of lymphocytic cells, which in turn disrupt the integrity of the myelin sheath (Filippi et al., 2018). Additionally, it is associated with alterations in microvascular perfusion (changes in blood flow within small blood vessels)(Law et al., 2004; Y. Lin et al., 2012). Furthermore, maintaining adequate cerebral perfusion appears to be crucial for the successful process of remyelination in MS (Law et al., 2004).

The perfusion in NAWM is believed to be decreasing, both globally and at the capillary level, in individuals with relapsing-remitting multiple sclerosis (RRMS) (Law et al., 2004). Furthermore, this capillary-associated hypoperfusion is linked to a decline in the microstructural integrity of white matter in RRMS patients (Sisco et al., 2021). Evolving evidence from perfusion-weighted imaging studies suggest that cerebral hypoperfusion in patients with multiple sclerosis can be present from the early beginning to more advanced disease stages, and it could be associated with chronic hypoxia, focal lesion formation, diffuse axonal degeneration, cognitive dysfunction, and fatigue. (D'Haeseleer et al., 2015).

Dynamic susceptibility contrast (DSC) magnetic resonance imaging (MRI) is a valuable tool for quantitatively evaluating cerebral perfusion, particularly during the acute inflammatory phase of lesion development in multiple sclerosis (MS) (Sheng et al., 2019). Using DSC-MRI, researchers have observed both increases and decreases in global perfusion, reflecting the complex spatial and temporal dynamics seen in relapsing-remitting MS (RRMS). In areas of normal-appearing white matter (NAWM), hypoperfusion has been linked to persistent low-grade inflammation, metabolic or vascular issues, or primary ischemia (Ge et al., 2005; Sowa et al., 2015). Conversely, heightened perfusion before the formation of focal white matter lesions has been observed (Peruzzo et al., 2013; Wuerfel et al., 2004), and could either be linked to an increased inflammatory response or a response to primitive hypoxic focal injury of the tissue. Therefore, the transient hyper-perfusion preceded the onset of hypoperfusion in the prelesion and subsequently in the established lesion.

The demyelination processes inherent in this disease are also linked to a condition of pseudo-tissue hypoxia (Trapp & Stys, 2009). This state may arise due to an imbalance between the heightened energy demand of neurons, particularly driven by a reorganization of ion channel distribution on axons, and the compromised supply of oxygen and glucose to anatomical areas in the white matter that are naturally poorly perfused (Trapp & Stys, 2009). Molecular evidence suggests that the hypoxic state is not a late consequence of demyelination but occurs early in lesion formation (Halder & Milner, 2021; Juurlink, 2013). Imaging studies demonstrating

hypoperfusion in patients with multiple sclerosis have revealed regional anatomical heterogeneities (Law et al., 2004). Interestingly, it has been demonstrated that transiently, approximately three weeks before the appearance of contrast enhancement (which serves as a reference for the radiological zero moment of lesion birth), transient hyper-perfusion could be observed in some pre-lesions (Wuerfel et al., 2004). This hyper-perfusion preceded the onset of hypoperfusion in the prelesion and subsequently in the established lesion.

However, the relationship of these perfusion variations with the demyelination state within the white matter remains unexplored as of yet. The gadolinium enhanced that is seen in the first three week of lesion formation is known to be due to the BBB increase of permeability and makes hard to specifically study the variation of blood influx, since there is a leakage of intermediate molecules.

Chapter 2 -

PET

The Positron Emission Tomography, also known as PET, is a nuclear medical imaging technique which measures the concentration of radioactivity in a 3D volume over time. It requires a scanner for the image acquisition and a cyclotron for radiolabelled molecules production. This instrumentation can be found inside the nuclear medicine department.

Disease mechanisms can be investigated in preclinical models and patients with multiple sclerosis by imaging techniques (e.g., PET and MRI). This work will focus just on the PET, that enables the acquisition of in vivo measurements of specific mechanism that contribute to neuro-axonal damage and loss in multiple sclerosis (MS). A deep understanding of the mechanisms underlying this process is a prerequisite for the advancement of treatment targeted at progressive MS.

2.1 PET imaging in MS pathophysiology

The interest in assessing the in vivo dynamics of myelin loss and regeneration in multiple sclerosis (MS), as well as the impact of pro-myelinating compounds in patients with this condition, has created a demand for new imaging metrics that are both highly sensitive and specifically geared toward myelin content. While conventional T2-weighted MRI is proficient at identifying white matter lesions in MS due to its sensitivity, it lacks specificity for elucidating the underlying pathological substrates associated with these lesions. To address this issue, several imaging techniques have been developed to measure changes in myelin content in vivo. These techniques rely on the utilization of positron emission tomography and quantitative MRI methods. PET image has an inherent molecular specificity that allows the quantification of several key biological process, such as neuroinflammation, astrocyte activation, demyelination, remyelination, energetic dysregulation and neural damage. These processes can be characterized in terms of their regional localization in the brain, their temporal courses, their interactions, and their effects on neurological disability and neuro-axonal damage (Bodini et al., 2021). Through the combined use of PET and MRI, significant unanswered questions regarding the physiopathology of multiple sclerosis (MS) may become resolvable through

clinical investigations. Ultimately, this could empower clinical trials to target the fundamental processes underlying clinical progression in MS.

Prolonged activation of microglia, the resident immune cells in the brain, have been associated with pathological progression of neurodegenerative disorders, including multiple sclerosis (Nutma et al., 2019).

Our understanding of how macrophages and microglia contribute to neurodegeneration in multiple sclerosis (MS) has significantly advanced since the introduction of PET imaging with radiolabeled compounds specifically targeting the 18-kDa translocator protein (TSPO). TSPO is situated on the outer mitochondrial membrane, and increased TSPO levels correlate with a higher density of activated macrophages and microglia in the context of MS (Banati et al., 2000; Nutma et al., 2019). The foremost insight derived from the application of TSPO PET in multiple sclerosis (MS) is that the involvement of microglia and macrophages in the pathogenesis of the disease extends beyond the progressive phases; it is integral to the pathology right from the disease's onset (Banati et al., 2000; García-Lorenzo et al., 2018; Politis et al., 2012; Rissanen et al., 2014). In comparison to the binding of TSPO tracers in healthy individuals, elevated binding has been observed in lesions, areas surrounding lesions, and in both normal-appearing white and grey matter in MS patients across all stages of the disease. These binding levels are also correlated with clinical and cognitive parameters (Banati et al., 2000; Giannetti et al., 2015; Hagens et al., 2018; Rissanen et al., 2014).

PET imaging with TSPO tracers is expected to maintain its significance in the study of neuroinflammation in multiple sclerosis (MS) in the foreseeable future. Indeed, TSPO PET is poised to play a crucial role in evaluating novel treatments aimed at halting disease progression by regulating the activation of innate immune cells, including the use of Bruton's tyrosine kinase inhibitors (Montalban et al., 2019).

2.2 General principles of PET

PET enables quantification of different biological process, like blood flow, metabolism, and protein concentrations, using radiotracers. This functional imaging technology aligns exceptionally well with the three principles of tracer measurements. PET instrumentation allows precise quantification, PET labels maintain tracer properties unaltered, and PET ligands are present in minute concentrations. These attributes stem from the unique capability of the

technology to utilize high-energy radiation emitted from the nucleus, in contrast to low-energy modes such as computed tomography, where X-rays are emitted by orbiting electrons (Turkheimer et al., 2015). In contrast to anatomical imaging methods like X-ray, ultrasound, and magnetic resonance imaging (MRI), PET provides real-time insight into biological processes at the molecular level. This is achieved through the utilization of a specific ligand carrying a positron-emitting radionuclide, known as a PET tracer. This unique feature grants PET technology exceptional sensitivity and excellent tissue penetration (Huang et al., 2020).

Radionuclides, also known as radioactive isotopes or radioactive atoms, are unstable forms of elements that emit radiation as they decay. These radioactive atoms are used to label molecules and create radioligands or radiotracers for PET imaging. Choosing one over another requires carefully studying one type of metabolism over another.

However, the currently available radioligands still do not encompass all the required target of interest in MS. This includes cells families like oligodendrocytes, or lymphocytes, as well as the ability to discriminate between different cell phenotypes, such as pro-inflammatory and anti-inflammatory microglia. Furthermore, even if a target is identified, PET radiotracer must fulfil a wide range of rigorous criteria to be deemed appropriate for assessing pathological alterations in humans.

A typical dynamic PET acquisition consists of the injection of a specific dose of radiotracer into the patient, followed by measurement of the decay activity of the radionuclide. The radioactivity in both the bloodstream and in the organ of interest is monitored throughout the experiment, generally lasting an hour or more.

The two traditional PET experimental frameworks are static (single-frame acquisition) and dynamic (multi-frame acquisition). Due to its practicality, static PET imaging is primarily used for clinical applications (reasonable costs and easy patient management). Ninety percent of all annual PET scans are performed in oncological and cardiac imaging, the main applications (Bertoldo et al., 2014). Dynamic PET studies are instead used in research and in particular neuroscience research and include multi-frame pictures taken from the time of tracer injection for up to 60-90 minutes. PET remains the gold standard for examining tissue metabolism despite the recent development of magnetic resonance imaging. Blood sample is frequently used in conjunction with dynamic investigations, which is one of the most significant restrictions on the application of these tests in ordinary clinical practice. By using kinetic

modeling, quantitative measures can be obtained with dynamic PET, but it is more expense and is more time-consuming. The fundamental benefit of these measurements is that they are proportional to the relevant biological variable's underlying value.

2.3 Compartmental models

Moving from static to more informative dynamic PET acquisition, three model classes represent the most frequently used approaches: compartmental models, the spectral analysis modelling approach, and graphical methods. In this work we will focus in the first model.

The most difficult phase of quantitative PET is compartmental modeling (Cobelli et al., 2002), which aims to reveal the mechanism of the system under investigation. Compartmental modeling demands a complete mathematical description of the system processes, in contrast to the other quantitative approaches mentioned above. Therefore, the only method that enables a thorough knowledge of the physiological system itself and/or of the pathophysiology of a disease is compartmental modeling. Notably, compartmental modeling serves as the foundation for PET quantification. This is due to the fact that all of the above-mentioned simpler quantitative techniques are based on a compartmental description of the PET tracer dynamics.

Dr. Sokoloff and colleagues (Sokoloff et al., 1977) in 1977 established the theoretical basis of the well-known two-tissue compartment model used to quantify [^{18}F] FDG brain studies. Since then, compartment models have played a significant role in quantitative PET imaging. The most significant and pertinent models used in PET to derive and quantify physiological information in absolute measurement units are Sokoloff's model, the one-tissue two-parameter model for the quantitative assessment of blood perfusion, and the two-tissue four-parameter model for receptor ligand binding studies (Bertoldo et al., 2014). The last one, represented in Figure 2.1, is the gold standard model for the estimation of the K_1.

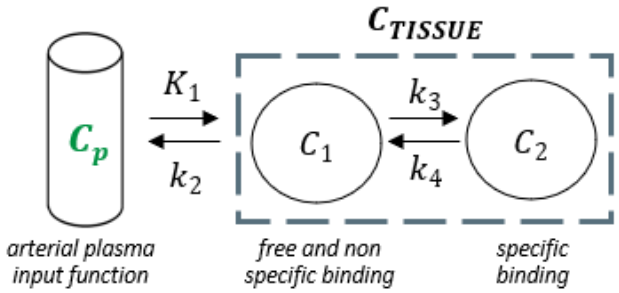

***Figure 2.1 Gold standard compartmental model for the estimation of the K_1**: The first compartment is the arterial blood. From arterial blood, the radioligand passes into the second compartment, known as the free and non-specific binding compartment. The third compartment is the region of specific binding.*

The model parameters (K_1, k_2, k_3, and k_4 in Fig. 2.1), usually referred to in PET literature as microparameters, can be estimated with the help of dynamic PET images and arterial plasma samples. It should be noted that K_1 is frequently published in the PET literature with a capital K to indicate a distinct unit of measurement ($ml/cm^3/min$ or $ml_{plasma}/ml_{tissue}/min$) from those of the other microparameters in Fig. 2.1 (min^{-1}).

Quantitative procedures are appropriate for research PET investigations but often inapplicable for clinical studies, when simpler approaches are required, due to their complexity (dynamic PET imaging and blood measures). Complete quantification of the targets of interest requires measurement of tracer concentrations in the arterial plasma throughout the entire scan duration (Hooker & Carson, 2019). However, this approach is invasive and demanding, particularly for patients with disabilities (Tonietto et al., 2016).

2.4 TSPO imaging with PET

For what concern neurodegenerative disorders PET is a powerful tool for the in vivo characterization of neuroinflammation process. In response to various stimuli, as well as neurodegenerative and psychiatric diseases, the 18-kDA translocator protein (TSPO) is consistently elevated in activated microglia of the central nervous system (CNS) (Turkheimer et al., 2015). It is therefore a target of interest for molecular strategies aimed at imaging neuroinflammation in vivo.

For the past 20 years or so, the antagonist ligand PK11195, an isoquinoline-carboxamide derivative, has been used in PET imaging of the TSPO (at the time still known as the peripheral

benzodiazepine receptor, or PBR). PK11195, labelled with 11 C, was used to target the TSPO in activated microglia and invading macrophages in the central nervous system (CNS) after initially being applied to the imaging of the TSPO in the heart (Charbonneau et al., 1986). Nonetheless, [^{11}C]PK11195 exhibits a relatively low signal-to-noise ratio (SNR) primarily because of its pronounced nonspecific binding. Additionally, the short half-life of ^{11}C, which is only 20.4 minutes, constrains its broad applicability in terms of transportation and clinical trials (Zhang et al., 2021).

The growing evidence that neuroinflammation is a significant contributor to disease and the resulting interest in CNS immune system biomarkers brough to the development of PET imaging of the TSPO with second generation radioligands. The aim was to improve the quality of TSPO imaging through novel radioligands with higher affinity and more accurate visualization of TSPO (Datta et al., 2017; Vignal et al., 2018). Novel series of phenoxyphenyl acetamide derivatives (i.e., PBR06, DAA1106) or bicyclic linker derivatives (i.e., PBR111, DPA713) with high affinity for the TSPO have been radiolabelled for use in PET with the aim of improving the signal-to-nose properties of [^{11}C] -(R)-PK11195 (Charbonneau et al., 1986).

Although these novel PET tracers exhibit enhanced signal-to-noise ratios (SNR), a limitation arises from the variability in TSPO binding potential (BP) among individuals, which is attributed to a single nucleotide polymorphism in the TSPO gene (Fan et al., 2015). The human TSPO gene, found on chromosome 22q13.3, comprises four exons and encodes 169 amino acids (Lin et al., 1993). Recent research has identified a specific single-nucleotide polymorphism (rs6971) in exon 4 of the human TSPO gene, leading to a nonconservative alanine-to-threonine substitution that affects the ligand binding affinity of the TSPO protein (Kreisl et al., 2013). The rs6971 polymorphism can result in three distinct binding statuses: high-affinity, mixed-affinity, and low-affinity binders. It's worth noting that all second-generation TSPO tracers are susceptible to a prevalent polymorphism (rs6971) in the TSPO gene, and this polymorphism has a discernible impact on the in vivo affinity of these tracers (Zhang et al., 2021). As a result, it is necessary to genotype individuals before they undergo TSPO PET scans. This genotyping helps identify whether they express the TSPO form that exhibits high affinity binding to the tracer, the form with low affinity, or a combination of both. These different genotypes produce distinct PET signals despite having similar TSPO levels (Zhang et al., 2021). Currently, individuals who exclusively express the low-affinity form of TSPO must be excluded from TSPO PET studies due to the insufficient signal-to-noise ratio it

generates. The prevalence of these polymorphisms varies depending on ethnic backgrounds, with LAB frequency ranging from approximately 1 in 10 Caucasians to roughly 10 times less common in East Asians. Specifically, this group comprises approximately 9% of individuals of European, Middle Eastern, and North African ancestry, around 6% of the African American population, and a notably smaller percentage, specifically 0.001%, of the Han Chinese population (Owen et al., 2012). Therefore, the development of novel radioligand candidates that are insensitive to the rs6971 polymorphism, specifically third-generation PET tracers, would expand the pool of eligible participants for TSPO imaging in human studies (Zhang et al., 2021).

Finally, TSPO plays a pivotal role in facilitating the movement of cholesterol from the outer to the inner mitochondrial membrane, consequently regulating the pace of neurosteroid production. Furthermore, TSPO is implicated in various other physiological processes (Larcher et al., 1989; Veenman & Gavish, 2006). Nonetheless, TSPO has been demonstrated to participate in conditions such as brain ischemia-reperfusion injury (Pulagam et al., 2017), neurodegenerative disorders (Papadopoulos et al., 2006), and several other diseases (Leonelli et al., 2005; Veenman et al., 2002). Within the central nervous system (CNS), TSPO expression undergoes a significant upregulation in activated microglial cells in response to inflammatory stimuli (Knezevic & Mizrahi, 2018). In their study, Lavisse et al. (Lavisse et al., 2012) discovered that reactive astrocytes also exhibit an elevated expression of TSPO. Moreover, there are instances where activated peripheral macrophages express TSPO (Dupont et al., 2017). In theory, in situations where the blood-brain barrier (BBB) is compromised, these peripheral macrophages could potentially infiltrate the brain. The abnormal expression of TSPO in glial cells (Cosenza-Nashat et al., 2009; Venneti et al., 2008) is implicated in the progression of neuropsychiatric disorders associated with neuroinflammation. This includes conditions like Alzheimer's disease (AD), amyotrophic lateral sclerosis (ALS), Parkinson's disease (PD), and multiple sclerosis (MS) (Cosenza-Nashat et al., 2009; Venneti et al., 2008). Consequently, TSPO is regarded as a promising biomarker for neuroinflammation, offering potential utility in assessing the efficacy of anti-inflammatory treatments (Gershen et al., 2015; Setiawan et al., 2015).

A significant limitation of TSPO PET in multiple sclerosis (MS) is that TSPO expression is not entirely specific to actively engaged innate immune cells. There is an ongoing debate regarding whether TSPO is upregulated by human microglia upon their activation (Nutma et al., 2021;

Owen et al., 2017). Furthermore, while the majority of cells expressing TSPO in MS appear to be macrophages and microglia, activated astrocytes and, to a lesser extent, endothelial cells also contribute significantly to TSPO expression (Nutma et al., 2019). Additionally, TSPO expression does not discriminate between innate immune cells with a pro-inflammatory profile and those with an anti-inflammatory profile (Bonsack et al., 2016). This knowledge is crucial for investigating the effects of drugs on modulating the profiles of innate immune cells.

Chapter 3 -

MATHERIALS AND METHODS

All model fitting and statistical analyses were performed using the MATLAB 2022b (Mathworks).

3.1 Methodological framework

The current standard for the quantification of the influx rate constant for TSPO PET tracers is the use of the reversible two-tissues compartmental model, with metabolite corrected plasma input function, to fit the tissue whole-dynamic time activity curve (2T4K-C_p, Figure 3.1a).

In this work it has been used a simplified quantification approach consisting in the estimation of the K_1 kinetic parameter via fitting of the first minutes of the tracer kinetic in the tissue.

In order to derive a completely non-invasive procedure, the method relies on 3 different hypotheses:

1. Within the first minutes after the injection, it is reasonable to assume that exchanges between the first and the second compartment and the venous efflux have not yet occurred, or if it is so, that their effect on the dynamics is negligible. In this framework, the kinetic of the tracer is mostly reflecting the tracer influx from blood to the parenchyma and we can think to reduce the two tissues irreversible compartments model to a model with only one irreversible compartment. Model equation can be furtherly simplified through the deletion of the parametrization of the fraction of blood volume ($V_b = 0$), which brings to the definition of a linear model for the estimation of K_1 parameter (1T1K-C_p, Figure 3.1b). To note, while usually applied in the context of parametric mapping [REF?], assuming a null V_b represents a relevant approximation if applied to region of interest (ROI) analysis.
2. In a limited time-window after tracer injection, the production of metabolites from the parent radiotracers is still limited. In the case of many PET tracers, it is possible to identify a specific time window after tracer injection in which the impact of the metabolites on the parent plasma fraction is still negligible (<10%) as compared to the total parent. By ignoring the production of metabolites and uneven tracer distribution

between red-blood cell and plasma, we can assume the whole blood tracer concentration as a reasonable approximation of the parent plasma tracer concentration and use it as input function of the model (1T1K-Cb, Figure 3.1c).

3. In this framework, by the adoption of a robust protocol for IDIF extraction and by assuming that the computed IDIF is a good approximation of the whole blood tracer activity, it can be adopted as input function of the compartmental model (1T1K-IDIF, Figure 1d), bringing to the definition of a completely blood-free method for the estimation of the K1 parameter.

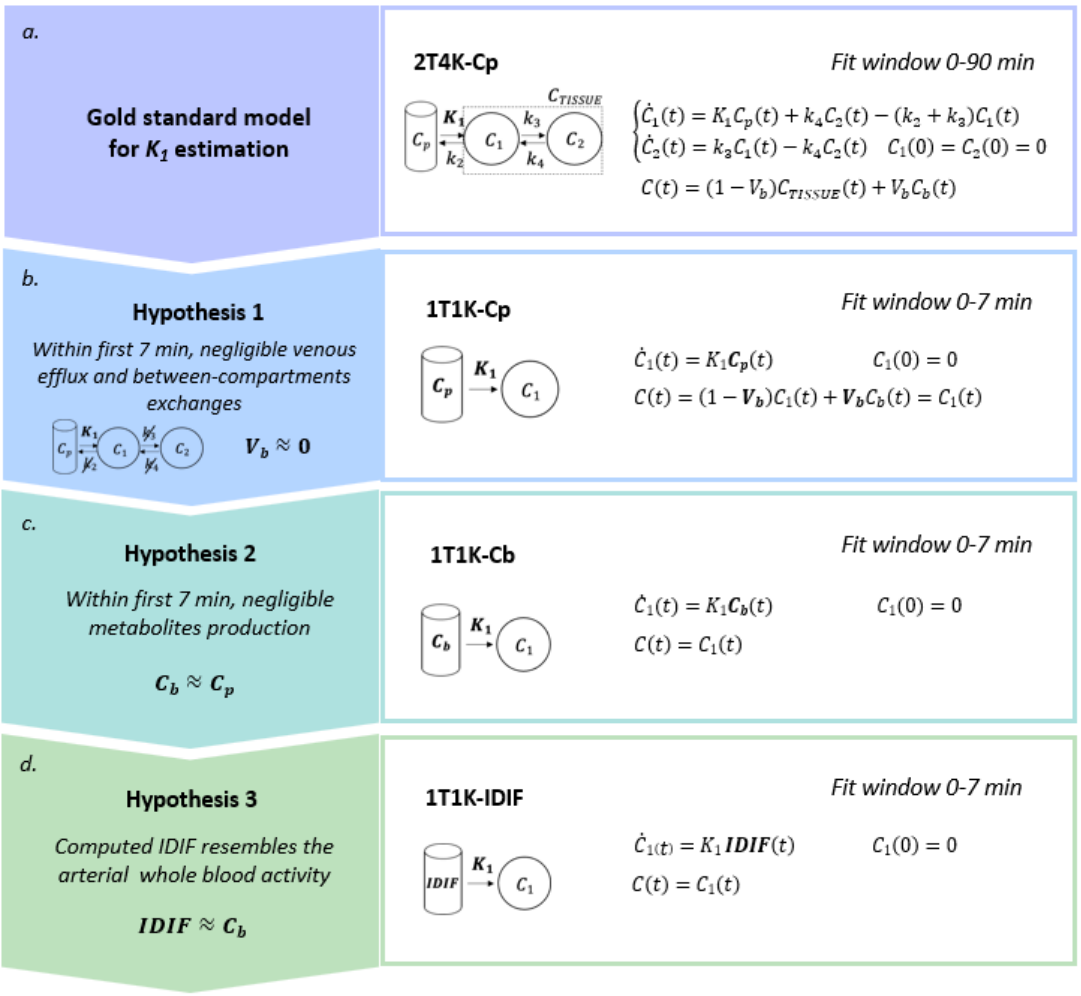

Figure 3.1: Development of a simplified blood-free methodological framework for K1 estimation: *panel a shows the gold standard compartmental model for kinetic modelling of TSPO radiotracers; panels b, c, d show the simplified models for the K_1 estimation derived when considering a limited time window of around 7 minutes for model fitting.*

3.2 Study participants and data acquisition

The study comprises one hundred and one subjects using three different protocols. The first protocol involves twenty-two multiple sclerosis patients, with twenty-three matched healthy controls (fifteen images from the tests and eight from the retests). The remaining two protocols consist of by forty-one and fifteen healthy controls, respectively. All the images have been acquired from the same machine.

Written informed consent was obtained from all participants, and the protocols were approved by the Medical Bioethics Committee of Ile de France Region and in accordance with French legislation and the Declaration of Helsinki 1975 (and revised in 1983). All subjects were considered healthy according to their medical history record and physical examination. They all had a normal brain MRI. Genomic DNA from blood samples was used to genotype the rs6971 polymorphism of the TSPO gene.

All PET imaging sessions were acquired with a continuous dynamic acquisition, from 0 to 90 min after a bolus injection of the tracer. For 8 participants, arterial blood data were sampled via radial artery catheter at the time of the scan and corrected for metabolites, just one of them had the scan during the re-test. PET data reconstruction varied across imaging sites and scanner types, but all included correction for random noise, scatter and tissue attenuation. All participants were genotyped for the rs6971 polymorphism of the TSPO gene prior to scanning, and only High Affinity Binding (HAB) and mixed affinity binders (MAB) were considered. With the purpose of tissue segmentation and region of interest (ROI) parcellation structural T1-weigheted (T1w) Magnetic Resonance (MR) images were also acquired for each participant. Studies were approved by local ethics committees and institutional revision boards prior to start, and all participants provided informed consent after a full description of the study.

	Numbers of subjects	**HAB**	**MAB**	**LAB**	**Age range**	**Age (mean ± SD)**	**Women**	**Men**
HC	79	42	30	7	23-60	59.62 ± 15.02	54	25
AIF	8	5	4	0	23-59	39.11 ± 13.04	5	3
MS	22	11	11	0	28-67	47.50 ± 9.85	14	8

Table 3.1: ***Dataset division:*** *the total amount of subjects is composed by the sixty-nine healthy controls and twenty-two multiple sclerosis patients. Eight of the healthy controls have the arterial input function (AIF).*

Images were acquired at Service Hospitalier Fre´de´ric Jolioand the Institut du cerveau et de la Moelle.

Each participant underwent a T1-weighted (T1-w) magnetic resonance image and an [^{18}F] DPA-714 PET acquisition (Lavisse et al., 2015). Eight subjects (five HABs, four MAB) underwent a second PET acquisition (injected activity difference $5.91 \pm 18.78\,MBq$) after five to three months to study the reproducibility of the quantification method.

T1-w imaging was performed using a turbo spin echo sequence (TSE) ($TE/TR = 3/6300\,ms$; alpha$= 10$, resolution $= 0.92\,x\,0.92\,x\,0.93\,mm$) in a 1.5T Philips Achieva (Best, The Netherlands) scanner or an MPRAGE ($TE/TI/TR = 2.98/900/2300$, alpha$= 9$, resolution$= 1\,x\,1\,x\,1.1\,mm$) in a 3T Siemens Trio scanner (Erlangen, Germany).

[^{18}F] DPA-714 was prepared according to standard conditions (Kuhnast et al., 2012). Subjects underwent [18F] DPA-714 PET scans in a high-resolution research tomograph (HRRT, Siemens, Knoxville, TN, USA). After a transmission scan using a ^{137}Cs point source, a [^{18}F] DPA-714 bolus was intravenously injected ($198.4 \pm 22.9MBq$). The dynamic PET acquisition in list mode lasted 90 min.

The eight subjects (five HABs and four MABs) with arterial input functions (AIFs) were corrected for metabolites (Lavisse et al., 2015).

PET acquisitions were corrected for random attenuation and scattered coincidences and reconstructed with the iterative-ordered subset expectation maximization (Ordinary Poisson [OP]-OSEM) 3D method (4 iterations using 16 subsets) including point spread function modeling within the reconstruction (using a 3D Gaussian kernel with 2 mm full-width at half-maximum). Dynamic data were binned into 27 frames ($6\,x\,1\,min, 7\,x\,2\,min, 14\,x\,5\,min$). Reconstructed dynamic PET data were realigned for motion correction using the frame-to-reference image registration in PMOD 3.5 (PMOD Technologies Ltd., Zurich, CH).

T1-w images were segmented using Freesurfer 5.3 (http://freesurfer.net) and regions of interest (ROIs) were selected: thalamus, hippocampus, cerebellar gray matter, white matter and occipital, parietal, frontal and cingulate cortices. A whole brain mask was also extracted. T1-w images and ROIs were resampled into the PET space using a rigid registration in order to extract TACs from each ROI. Data from the left and right hemispheres were averaged. Kinetic modeling (2-TCM) was performed using the COMKAT library and Logan graphical analysis was proceeded using in-house software in Matlab (Math Works, Natick, MA, USA).

3.3 Image derived input function and blood data analysis

A completely blood-free method for estimation of the K_1 parameter was applied to healthy subjects and multiple sclerosis patients.

The first step consisted of extracting all the TAC from the cortex and carotids of both healthy and MS subjects. Next, by averaging the carotid TACs of every voxel that resulted from the selection, the IDIFs were calculated. Since compartmental modelling relies on the assumption of a noise free input function, each IDIF was ultimately fitted.

The derived IDIF can be adopted as input function of the compartmental model (1T1k-IDIF), bringing to the definition of a completely blood-free method for the K_1 parameter estimation.

3.3.1 TACs extraction

The Time Activity Curves (TACs) were extracted by calculating the mean intensity value of pre-processed PET images within the ROI or voxel for the current frame. The result is the temporal variation of radiotracer uptake in specific regions of the brain over the course of multiple frames.

Whereas the carotid areas of healthy people were manually segmented, the ROIs for the cortex were taken using Free Surfer's masks. In the cortex, two distinct sets of ROIs were employed, each produced using a different mask. The first group, which consists of 148 ROIs from the cortex, left and right cerebellum, left and right thalamus, and the brain stem, has smaller volume ROIs. While the second group consists of 5 lobes of the cortex (frontal, insula, occipital, parietal, and temporal lobes), as well as the cerebellum grey matter, thalamus, and brain stem regions.

To ensure the right fit, the TACs were examined by the plot of SUV [g/ml] over the time [minutes]. To do it, the time activity curve was divided by the dosage over the weight to normalize all the TAC. The SUV [g/ml] was then calculated by dividing the obtained values by 1000.

3.3.2 Image derived input function (IDIF)

The arterial input function, i.e., the tracer's concentration in the arterial plasma (Cp), must be known for quantitative positron emission tomography (PET) brain research. Traditionally, it is performed via the invasive procedure of arterial cannulation. Although not harmful, arterial cannulation may make patients uncomfortable and deter patients and healthy volunteers from taking part in clinical research (Zanotti-Fregonara et al., 2011). Additionally, it is a laborious procedure for the research personnel the presence of radio-metabolites, i.e., radioactive molecules remaining in plasma that are formed by peripheral organs after tracer breakdown, makes it impossible to detect the C_p values directly (Tonietto et al., 2019). To get the parent concentration in plasma, C_p, the radio-metabolites concentration in plasma, C_{p_met}, needs to be adjusted using a chromatographic approach and then fitted with a mathematical model (Tonietto et al., 2016).

The practical limitations of arterial blood-based procedures have been addressed by several blood-free alternatives that have been presented in recent years. Among these, the raw blood time activity curves can be obtained by the image-derived input function (IDIF). This method is the one used in this work.

Carotid segmentation is the first stage in the IDIF calculation process. In the state of art carotid segmentation has been performed by both taking advantage of coregistrated magnetic resonance images (MRI) (Fung et al., 2009; Litton, 1997; Trebossen et al., 1999), and by placing carotid ROIs directly on PET images (Chen et al., 1998; Liptrot et al., 2004). However, in practice, it is challenging to achieve reliable MRI-base PET carotid segmentation. Moreover, the carotid is a tiny, elongated, and elastic structure that may be stretched, bent, and twisted according on how the head is positioned in relation to the body as a whole (Zanotti-Fregonara et al., 2011). Carotid segmentation performed directly on PET images seems to be a preferable choice since obviate the need to acquire an MRI and is not affected by coregistration issues. Furthermore, even if short-duration PET images have a low signal-to-noise ratio, which may make segmentation on these images challenging (Fung et al., 2009), carotids arteries are almost always easily recognizable on the early summed frames of a dynamic PET scan after a bolus injection of the tracer (Zanotti-Fregonara et al., 2011).

Techniques for segmenting the carotid arteries using PET scans can be automated or manual, and some of them rely on choosing a small number of hot voxels inside the carotid. These methods operate directly with dynamic PET data.

In the case of healthy controls, a manual segmentation of the internal carotids was already available. Given the manually segmented carotid mask and the dynamic PET images, syphon masks were extracted to derive the image derived input functions (IDIF).

The following steps were done to extract the siphon mask:

1. Identification of the mode peak among all voxels belonging to the mask using the calculated dynamic PET TACs in the carotid region.
2. Selection the dynamic PET volume corresponding to mode the peak time chosen.
3. Threshold at 20% of the maximum of the dynamic PET volume corresponding to the mode peak time within the mask.
4. Erosion and dilation (opening function) of the thresholded mask to remove isolated pixels.

Then, it is extracted the dynamic PET TACs from the voxels belonging to siphon mask.

Since compartmental modelling relies on the assumption of a noise free input function the IDIF for each subject was ultimately fitted using a linear regression for the rising part of the curve and a 3 exponentials model for the descending part of the curve.

3.3.3 Arterial Input Function

The arterial input function was tested on 8 healthy participants where we had the values of the C_p with and without the correction of metabolites, with the respective time frames. Therefore, the values of the Cb were missing. By following the second hypothesis of the employed model, i.e., not taking into account metabolite production, the value of C_b that was used in this thesis is the value of Cp without metabolite correction.

The following steps were done to organize the data:

1. Negative values are eliminated, and zero is used as the time's initial value.
2. If the time was less than 90, it was performed an extrapolation.
3. Create a virtual timeline from 0 to 90 in steps of 1/60.
4. Using the constructed virtual timeline, it was performed an interpolation of the values Cp and Cb.

3.3.4 K1 extraction

Once that the TACs and the fit IDIFs were extracted, it possible to calculate the K_1 [ml/cm^3/min]. The blood to brain influx constant has the following formula:

$$K_1 = FE$$

$$E = 1 - e^{-\frac{PS}{F}}$$

Where F is the cerebral blood perfusion [ml/cm^3/min], E is the unidirectional extraction fraction from blood into brain, during the tracer's first pass through the capillary bed, and PS is the permeability surface product, so is the product of capillary permeability P (cm/min) and capillary surface area S (cm^2/cm^3) (Crone, 1963; Renkin E. M., 1959). If:

$$PS >> F \quad \rightarrow \quad E \approx 1$$

Taking in consideration the gold standard compartmental model for the estimation of the k_1 (Fig. 3.1), the tissue time activity curve C_{PET} is calculated using the following formula:

$$C_{PET}(t) = (1 - V_b)C_{TISSUE}(t) + V_b C_b(t),$$

where C_b is the whole blood concentration, and V_b is the volume distribution [ml cm^3].

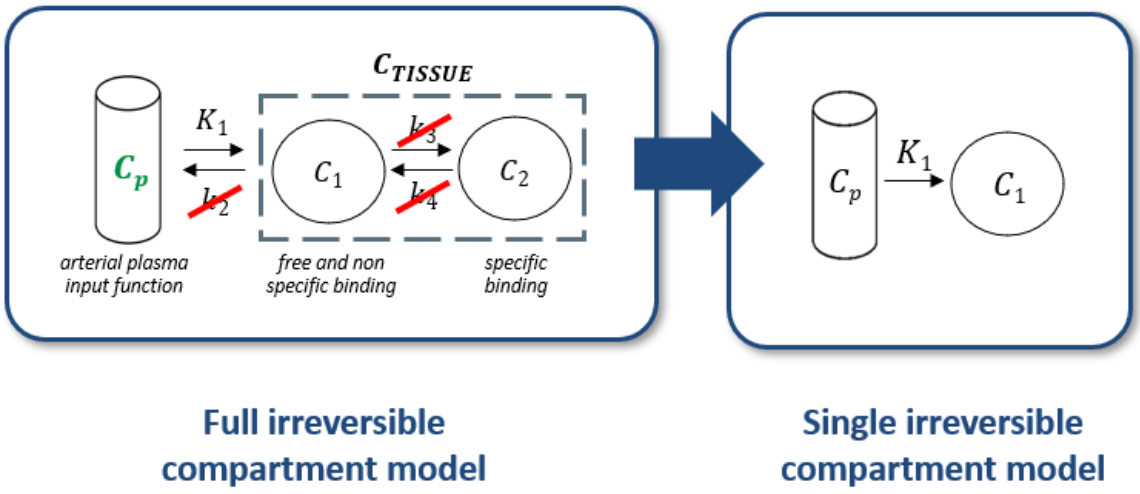

Figure 3.2 Full and reduced compartmental models: *it is possible to follow the model's hypothesis after the first seven minutes, being able to achieve the single irreversible compartmental model (in this figure it was taking in consideration just the input function C_b).*

Within the first seven minutes, it is possible to follow the hypothesis of the model. Following the first hypothesis the microparameters k_2, k_3, and k_4, in Fig. 3.1 (previously shown), will be not considered as a result of negligible venous outflow and negligible exchanges with the second compartment. Then, taking in consideration the second hypothesis, V_b will be set to zero. Therefore, the tissue time activity curve C_{PET} became:

$$C_{PET}(t) = C_1(t),$$
$$\frac{dC_1(t)}{dt} = K_1\, C_p(t)$$

Lastly, the last hypothesis makes possible to have negligible metabolites, so negligible tracer uptake by the red blood cells. ($C_p = C_b$).

Once these hypotheses were set, it was calculated the K_1. For each subject's ROI, K_1 regional estimates were calculated, and bias introduced for each hypothesis of the proposed simplified technique was successively examined. For all the cases, the a priori definition of the time window to use for model fitting was necessary. Standard 2T4K-C_p K_1 estimates were finally computed, using the eight arterial input function, by fitting the whole 0-90min tracer kinetic using a weighted non-linear least-square estimator with weights chosen optimally as:

$$w_{ROI}(t_i) = dt_i C_{ROI}(t_i),$$

where t_i is the time instant, dt_i is the length of the scanning interval and $C_{ROI}(t_i)$ is the ROI average time activity at time t_i (Cobelli et al., 1982).

The K1 ratio was also estimated for each technique and each brain cortex ROI on the presumption that the cerebellar grey matter served as a pseudo-reference region.

$$R_1 = \frac{K_1}{K_{1,CER}}$$

Results were obtained with each of the three simplified approaches (1T1K-C_p, 1T1K-C_b, 1T1K-IDIF) using the image derived input function.

If the arterial input function was not present, the only output of the function is the 1T1K-IDIF.

3.4 A priori definition of the time window

Each frame aligns with a specific moment in the PET timeline (as outlined in Table 1). To decide the appropriate time interval for model fitting, it was conducted a priori determination of the time window. In order to do it, it was carried out both a sensitivity analysis and an assessment of metabolite production.

Frames	1	2	3	4	5	6	7	8
Time PET [min]	0.5	1.5	2.5	3.5	4.5	5.5	7	9

Table 1: For each frame there is the respective time PET with the window that it was taken into account.

3.4.1 Sensitivity analysis

Initially, the K_1 values from the eight subjects with arterial input function was extracted using three simplified methods (1T1K- C_p, 1T1K- C_b, 1T1K-IDIF) and the standard approach (2T4K- C_p K_1). The analysis began by employing a temporal window spanning from the first to the third frame. Subsequently, for each step, it was extended the time window to encompass up to eight frames.

For each frame within this time window progression, both absolute and relative biases ($bias$ and $relBias$) were computed. Additionally, it was calculated Pearson's coefficients of correlation, both within subjects (ρ_{intra}) and between subjects ($\rho_{between}$), for K_1 and R_1 estimates. Furthermore, the coefficient of variation (CV) for each frame in the process was determined.

3.4.2 Assessment of metabolites production

To conclude the sensitivity analysis and select the most suitable frame, the parent plasma fit was computed using interpolated valued of C_p and C_b. This was done using the following formula:

$$PPf = \frac{C_p}{C_b},$$

Where C_p is the whole blood concentration, and C_b is the parent plasma concentration.

Subsequently, plots illustrating the mean and standard deviation of the PPf were generated. These plots were created along the interpolated time using the data from the eight parent curves of the parent plasma fit.

3.5 Model validation

The assess the model's performance, it was conducted a comparison between K_1 estimates obtained from standard blood samples and K_1 estimates derived from the image derived input function.

3.5.1 Comparison with standard blood based K_1 estimates

The initial step in validating the proposed approach's performance in estimating the K_1 parameter involved a comparison with the standard reference method, 2T4K-C_p estimation. The data from the eight arterial input functions for this evaluation were used in this step. For each subject's region of interest (ROI), K_1 regional estimates were computed, and bias introduced for each hypothesis of the proposed simplified technique was successively examined.

First, using the real parent plasma as the input function, it was evaluated whether the one irreversible compartment applied to the early frames of the PET dynamics produced results similar to those of the entire compartmental model (1T1K-C_p K_1). Then, by computing the K_1 using the total blood input function, the hypothesis of negligible metabolite synthesis and red blood cell uptake was examined (1T1K-C_b K_1). To note, since information on the whole blood TACs was missing, the uncorrected plasma tracer concentration was adopted instead. Lastly, IDIF was used to compute regional K1 parameters as input to the simplified model (1T1K-IDIF K_1).

Results from each of the three streamlined approaches (1T1K-C_p, 1T1K-C_b, and 1T1K-IDIF) were compared to the corresponding standard 2T4K- C_p estimates in terms of ROIs K_1 and R_1 estimates by computing absolute and relative bias ($bias$ and $relBias$) and both intra-and between-subjects Pearson's coefficients of correlation ($\rho_{intra}, \rho_{between}$).

The following formulas were used to quantify the difference between an estimated value and the true or reference value, both in absolute terms (bias) and in relative terms (relative bias):

$$bias = full_{model} - reducted_{model}$$

$$relBias = \frac{full_{model} - reducted_{model}}{full_{model}} 100$$

3.6 Test-retest reproducibility of K_1 estimates

Regional 1T1K-IDIF K1 estimates were calculated for test and retest scans using a pool of 8 healthy individuals to evaluate the repeatability of the results. For each subject's test and retest scans, regions of interest (ROIs) were categorized into groups based on the brain's lobe location, including frontal, temporal, occipital, parietal, and insular lobes, and the brain's subcortical location, including cerebellum, thalamus, and brain stem. The average K1 estimates for each of these brain lobes were then computed.

To quantitatively assess the reproducibility of the results, the mean relative difference (MRD) of the regional K1 estimates was ultimately adopted. The MRD is a measure used to gauge the consistency or variability of the K1 estimations between the test and retest scans, providing insights into the repeatability of the data.

$$RD = \left(\frac{retest - test}{\frac{retest + test}{2}} \right) * 100$$

The calculated test and retest values for each subject were correlated with each other. This was done to examine the correlation between the test and retest measurements to assess the degree of agreement or consistency between these two sets of data. Correlation analysis helps determine how closely related or linearly associated the test and retest measurements are, providing insights into the reliability and stability of the measurements over time or across different conditions.

3.7 Regression model

A linear mixed-effects model was ultimately computed to describe the K1 (a parameter often associated with the rate of blood flow) in various brain lobes (frontal, insula, occipital, parietal, temporal) and subcortical regions (cerebellum, thalamus, brain stem). This model aimed to account for the influence of several factors, including the subjects' age, genotype classification, gender, the ratio between the administered dose adjusted for weight (DW), and the body mass index (BMI). DW and BMI were calculated in the following way:

$$DW = \frac{dose}{weight}$$

$$BMI = \frac{weight}{\left(\frac{height}{100}\right)^2}$$

In this analysis, four subjects were excluded because they lacked height data, and two were excluded due to missing weight data. Four other subjects were excluded because their genotype was low affinity binding (LAB). Consequently, the analysis was conducted on a dataset with sixty-nine observations. The linear mixed-effects model with six fixed-effect coefficients and 95% coefficient intervals (CIs) is based on the following formula:

$$K_1 \sim 1 + age + gender + genotype + DW + BMI$$

The estimated values, p-values, and R-squared (R^2) were then reported in a table, as detailed in paragraph 4.7 of your analysis.

Additionally, a step-wise regression analysis was employed, using the same physiological characteristics, to identify the subset of variables that most effectively explain the variance in the dependent variable.

These statistical analyses were carried out using MATLAB's 'fitlme' function for the linear mixed-effects model and the 'stepwiselm' function for the step-wise regression.

Finally, it was done a comparison between the K1 estimates and obtained significant

3.8 Comparison HC vs MS

The K_1 estimates of twenty-two patients with multiple sclerosis (MS), consisting of eleven with secondary progressive MS (SPMS), five with relapsing-remitting MS (RRMS), and six with primary progressive MS (PPMS), were compared with the cortex values in the healthy controls. Additionally, a comparison was made between the K_1 estimates in the white matter lesions and the normal-appearing white matter (NAWM).

3.8.1 Cerebral cortex

The Double Inversion Rate (DIR) technique, which is instrumental in visualizing lesions within the grey matter (GM), was not accessible for use. Additionally, a 7-tesla MRI was not available, which prevented the segmentation of cortical lesions. Consequently, the analysed grey matter cortex of the MS patients also includes lesions within it.

The K_1 estimate across subjects, and derived from the cerebral cortex, underwent a comparison between healthy controls and individuals with multiple sclerosis (MS). The clinical subtypes of multiple sclerosis were used to perform further analysis. Group differences were explored using an ANOVA test.

3.8.2 White matter and normal appearing white matter

Subsequently, binary masks for white matter and normal-appearing white matter were employed to extract K_1 values from each patient, and these values were sequentially compared using ANOVA as well. Differences along the clinical subtypes of multiple sclerosis were checked too.

Chapter 4 -

RESULTS

4.1 A priori definition of the time window

4.1.1 Sensitivity analysis

In between-subject correlation analyses, higher Pearson's coefficients were observed across all time windows when using the reduced models 1T1K-C_b and 1T1K-C_p. However, when IDIF was employed, the highest Pearson's coefficients were achieved using the first seven frames ($\rho_{between} = 0.66 \pm 0.12\%$) (Figure 4.1 a). As for the R1 estimates, independently from the input function adopted, similar values of between-subject correlation were observed in each time window. With an increase in the number of frames, the Pearson's coefficients tended to decrease until reaching the lowest values using the first seven frames ($\rho_{between} = 0.55 \pm 0.25\%$) (Figure 4.1 b).

For both K_1 and R_1 estimates, regardless of the input function, intra-subject correlation remained almost constant along the frames (Figure 4.1 c, d).

When IDIF is adopted, relative and absolute bias of K1 estimates decrease increasing the time window, meanwhile, using the reduced models 1T1K-C_b and 1T1K-C_p, the relative and absolute bias increases with an increase in the time window until reaching the largest time window (Figure 4.1 c, d).

Irrespective of the input function, the coefficient of variation (CV) showed a decreasing trend with an increase in the time window (Figure 4.1 g). It's worth noting that when IDIF was adopted, the coefficient of variation was consistently larger compared to when the reduced models 1T1K-C_b and 1T1K-C_p were used.

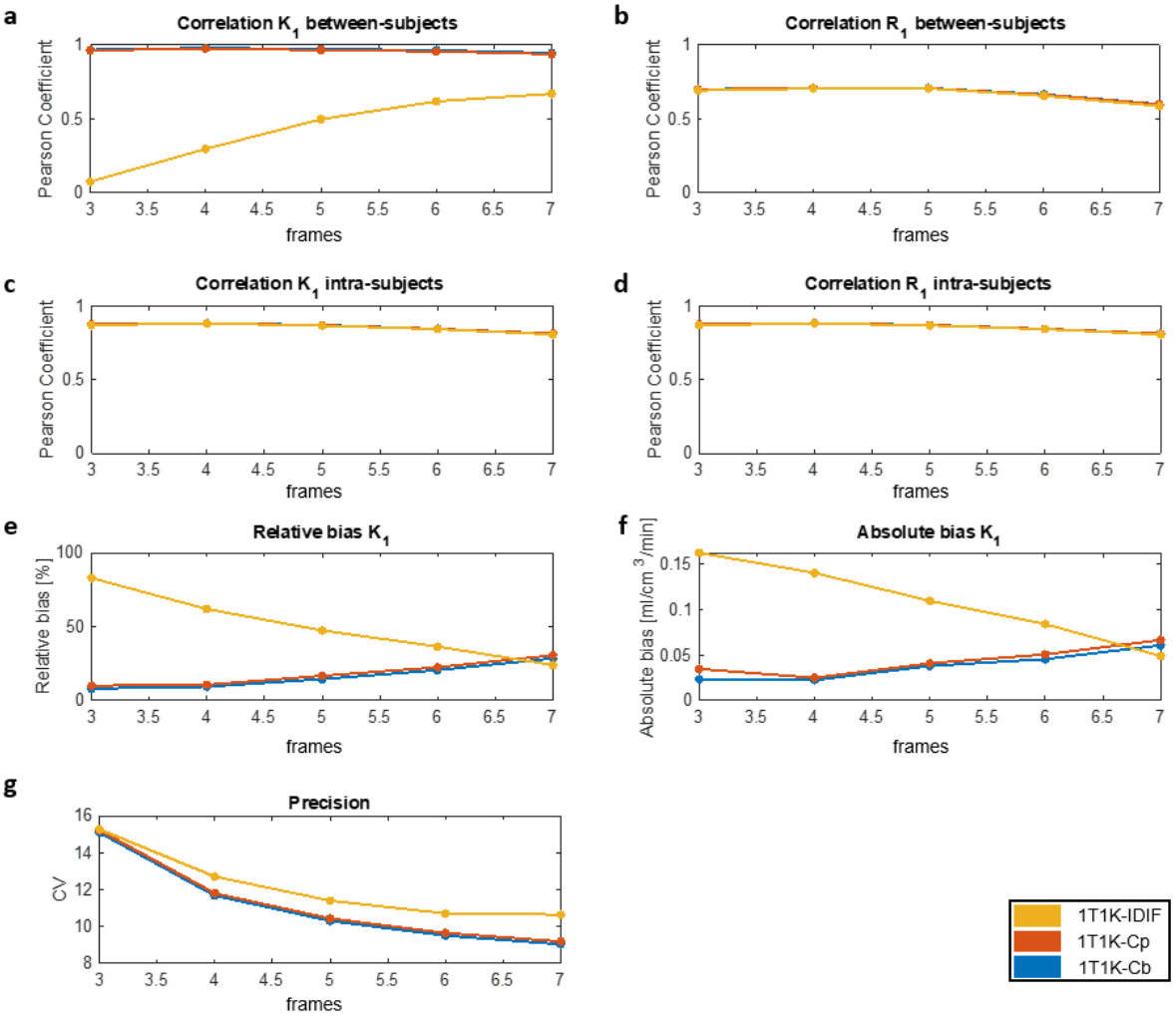

Figure 4.1. Comparison of ROIs K1 and R1 estimates, bias, and precision along different time window: panel a and b show, respectively for the *ROIs K_1 and R_1 estimates, the distribution of the between-subject Pearson's correlation coefficients between each of the reduced models (1T1K-C_p, 1T1K-C_b, 1T1K-IDIF) and the full model (2T4K-C_p). Panel c and d show, respectively for the ROIs K_1 and R_1 estimates, the distribution of the intra-subjects Pearson's correlation coefficients between each of the reduced models and the full model. Panel e and f show, respectively for the relative bias and absolute bias, the differences between the full and reduced model. Panel g show the coefficient of variation of the used model along the frames.*

4.1.2 Assessment of metabolites production

In accordance with the model's proposed hypothesis, the input function is the whole blood tracer, which is regarded as a reliable approximation of the parent plasma tracer concentration if the parent tracer is above 90% (within 8 minutes).

The a priori definition of the time window to be used for model fitting was required in each case. This decision was made as a result of a trade-off between the competing needs to include adequate samples for model fitting while keeping the model fit to a brief time window that respected the model hypotheses. In the end, this decision required to take into account variations in tracer kinetics, administration, and frame binning speeds for dynamic PET scans. After performing a sensitivity analysis and the assessment of metabolite production, it was selected the 7th frame, which corresponds to the 7th minute in the dynamic PET time frame and has a valued of $PPf = 0.9146$ (Figure 4.1). Therefore, compared to the entire parent plasma, the metabolites' influence on the parent plasma fraction is still minimal (10%).

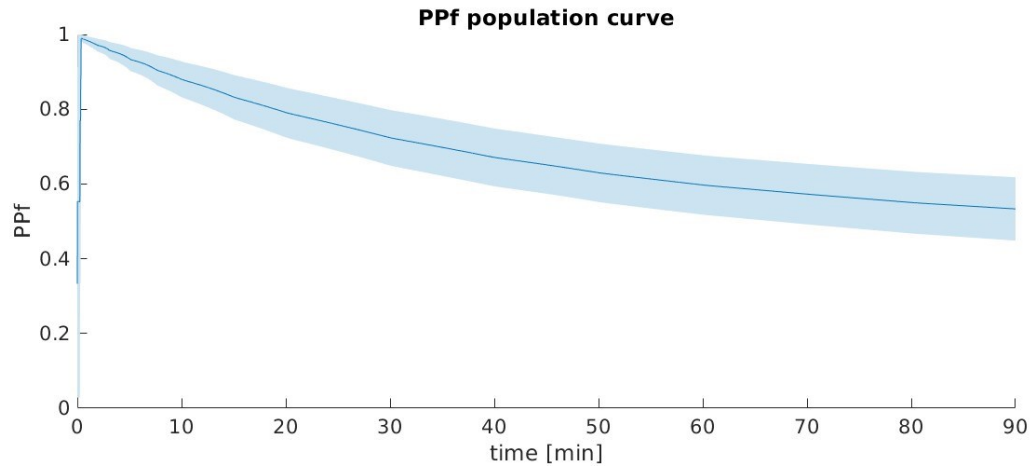

Figure 4.2: Parent Plasma fit (PPf) population curve for TSPO PET tracers. *Figure shows the mean (solid line) and standard deviation (shadowed band) of PPf curves for [18F] DPA714 in 8 healthy volunteers.*

Additionally, the beginning time (t_{start}) of this window was established for each participant at the point at which the mean grey matter TAC started to rise in order to account for potential pharmacokinetics variations with respect to the PET scan start time.

4.2 Model validation

4.2.1 Comparison with standard blood based K_1 estimates

Results of mean cortex K_1 and R_1 estimates are reported in Figure 4.3, together with Bland Altman plots in Figure 4.4, comparing the mean cortex 1T1K-C_p, 1T1K-C_b and 1T1K-IDIF to the reference 2T2K-C_p K_1 estimates. The highest bias is observed for the 1T1K-IDIF K_1 when compared with the ground truth 2T4K-C_p K_1 ($relBias$ = 7.21 ± 4.37%). Relative bias is maintained below 17.64% when comparing the 1T1K-C_p K_1 ($relBias$ = -27.82 ± 2.85%) and 1T1K-C_b K_1 ($relBias$ = -30.22 ± 2.76%) to the 2T4K-C_p K_1. As for the R_1 estimates, the relative bias is under 10.32% for all comparisons.

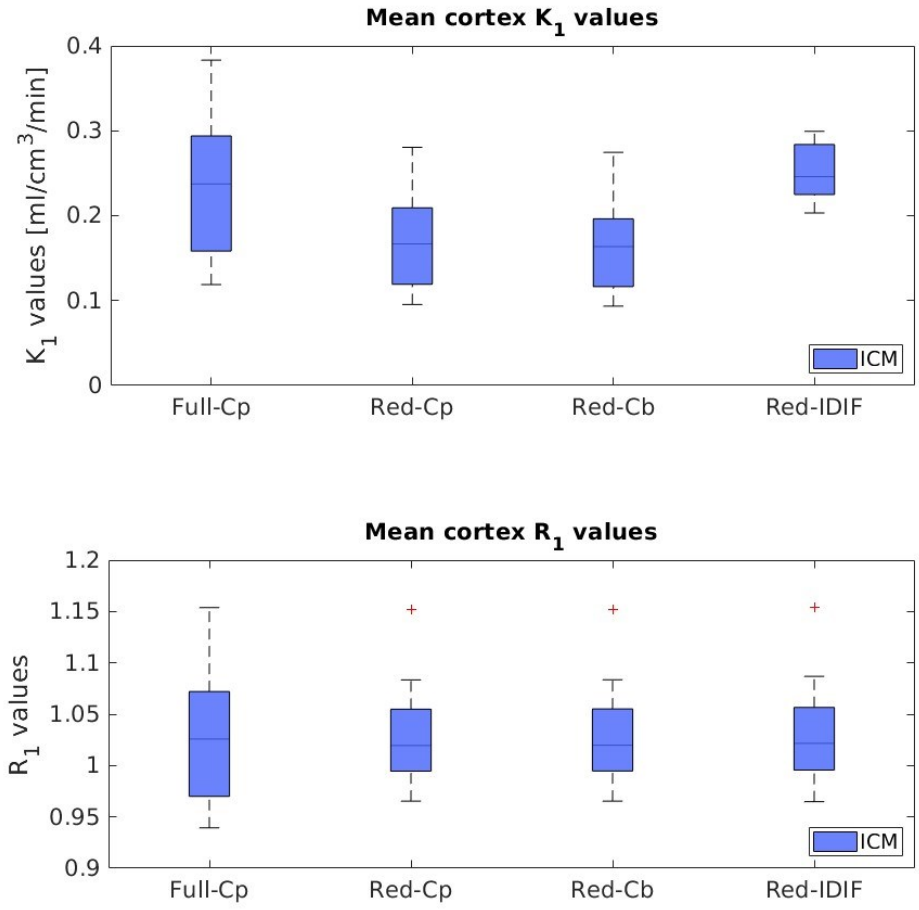

Figure 4.3: Comparison of mean cortex K1 and R1 estimates. *The upper and below panel show respectively the distribution across subjects of mean cortex K1 and R1 estimates computed via each of the aforementioned methods (2T4K-Cp, 1T1K-Cp, 1T1K-Cb, 1T1K-IDIF).*

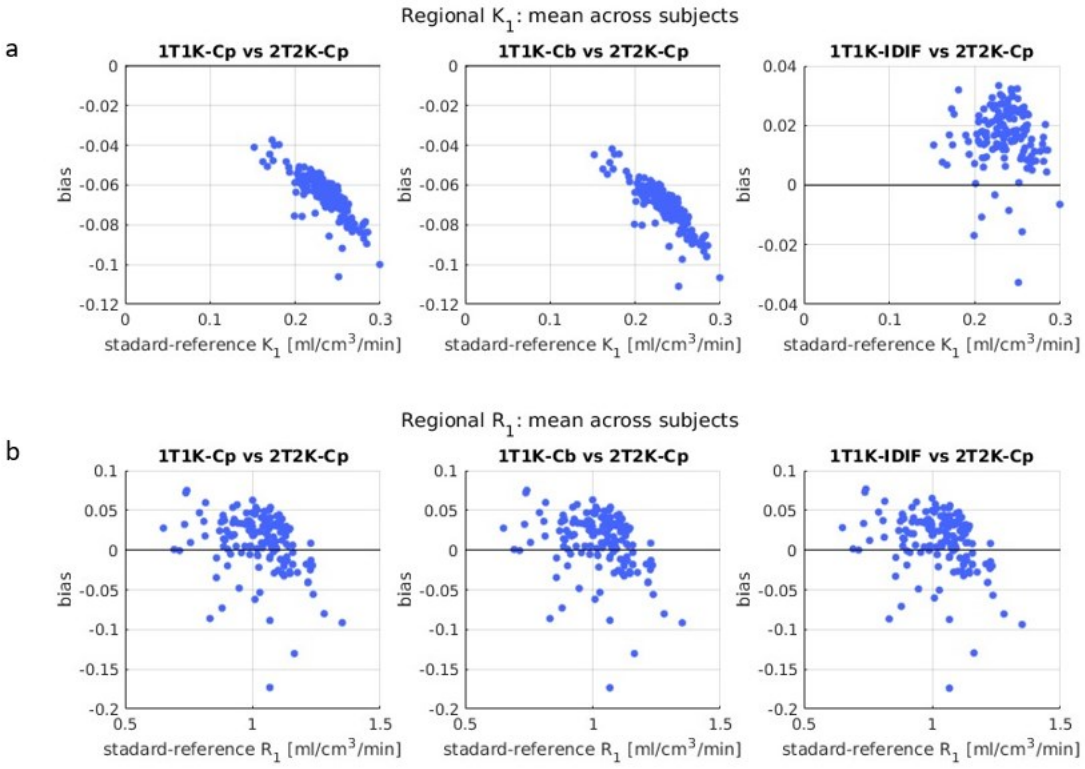

***Figure 4.4**: Panel a and b present Bland-Altman plots, which are used for the comparison between the outcomes of each of the simplified methodologies (1T1K-Cp, 1T1K-Cb, 1T1K-IDIF) and the standard-reference 2T4K-Cp estimates for both K1 and R1, respectively.*

Between-subjects correlation analyses show similar pattern to bias, with the lowest Pearson's coefficients reported when IDIF is adopted as input function of the model ($\rho_{between} = 0.66 \pm 0.12\%$). When comparing 1T1K-$C_b$ with 2T2K-C_p there is a high correlation ($\rho_{between} = 0.93 \pm 0.05\%$), and comparable results were found also for between subject correlation between 1T1K-C_p and 2T2K-C_p ($\rho_{between} = 0.93 \pm 0.05\%$), (Figure 4.5a). As for the R1 estimates, independently from the input function adopted, higher values of between-subjects correlation were ($\rho_{between} = 0.55 \pm 0.25\%$) (Figure 4.5b).

Independently from the input function adopted, intra-subjects correlation of both K_1 and R_1 estimates obtained with the simplified and full model result in mean above 0.79 (Figure 4.5c, d).

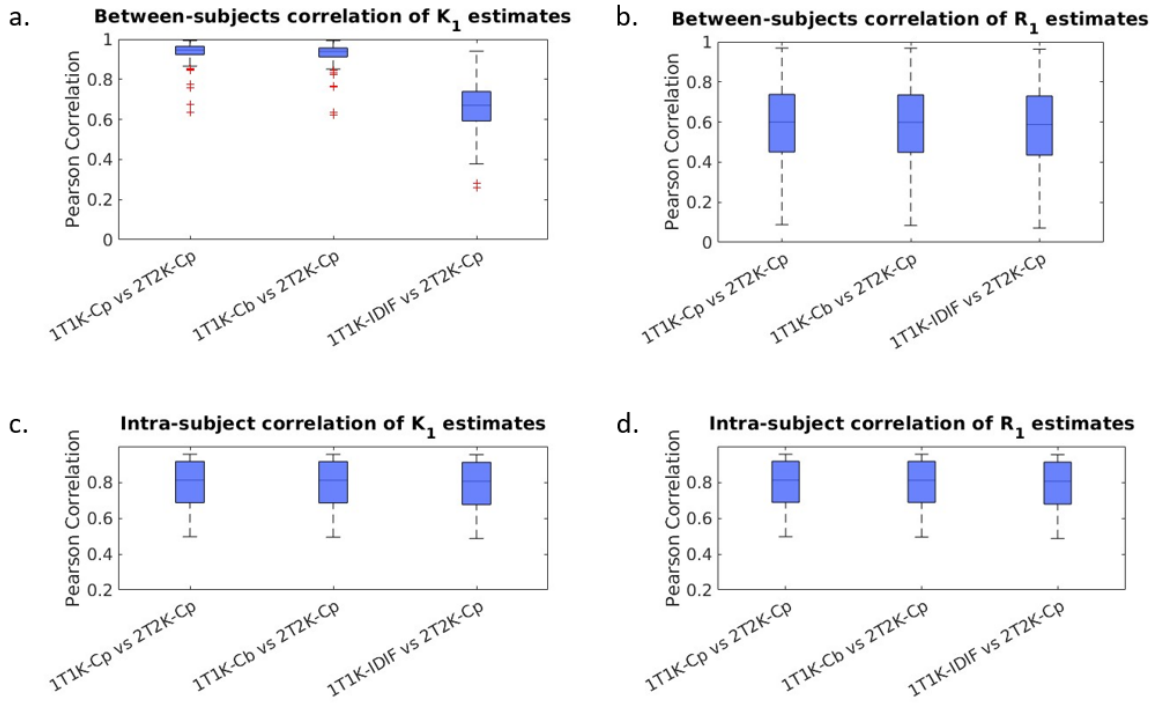

Figure 4.5. Comparison of ROIs K1 and R1 estimates: *panel a and b show, respectively for K_1 and R_1 estimates, the distribution of the intra-subject Pearson's correlation coefficients between each of the reduced models (1T1K-Cp, 1T1K-Cb, 1T1K-IDIF) and the full model (2T4K-C_p) ; panel c and d show, respectively for the ROIs K_1 and R_1 estimates, the distribution of the between-subjects Pearson's correlation coefficients between each of the reduced models and the full model.*

4.3 Test-retest reproducibility of K_1 estimates

High intra-subject correlation was reported for all the comparisons between test retest 1T1K-IDIF K_1 estimates ($\rho = 0.97 \pm 0.01$). The distribution of the subjects K_1 estimates, in five panels over eight, is upper than the dashed line of the bisector (Figure 4.6), meaning that K_1 estimates of the retest are higher than the ones of the test. This result is also visible in the Figure 4.7 and in the negative percentages of the MRD. In each subject, the physiological pattern of K_1 estimates is maintained along the region of interest (ROIs).

Mean relative difference across all the ROIs ($MRD = 9.19 \pm 20.95$). The standard deviation represents the variability or spread around this average difference, suggesting that there is a considerable amount of variation in the relative differences among the ROIs. This wide range of variation is worth further investigation and consideration when interpreting the results.

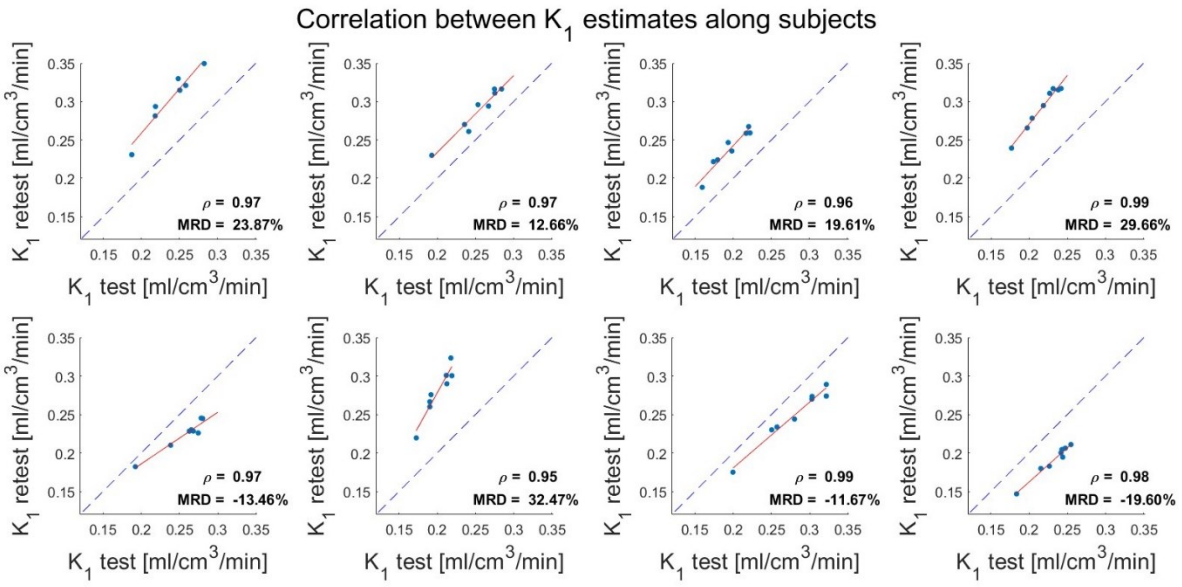

***Figure 4.6. Comparison of subjects K_1 estimates**: these panels show the distribution of the intra-subject Pearson's correlation coefficients between the test and retest of the reduced model 1T1K-IDIF K_1 estimates.*

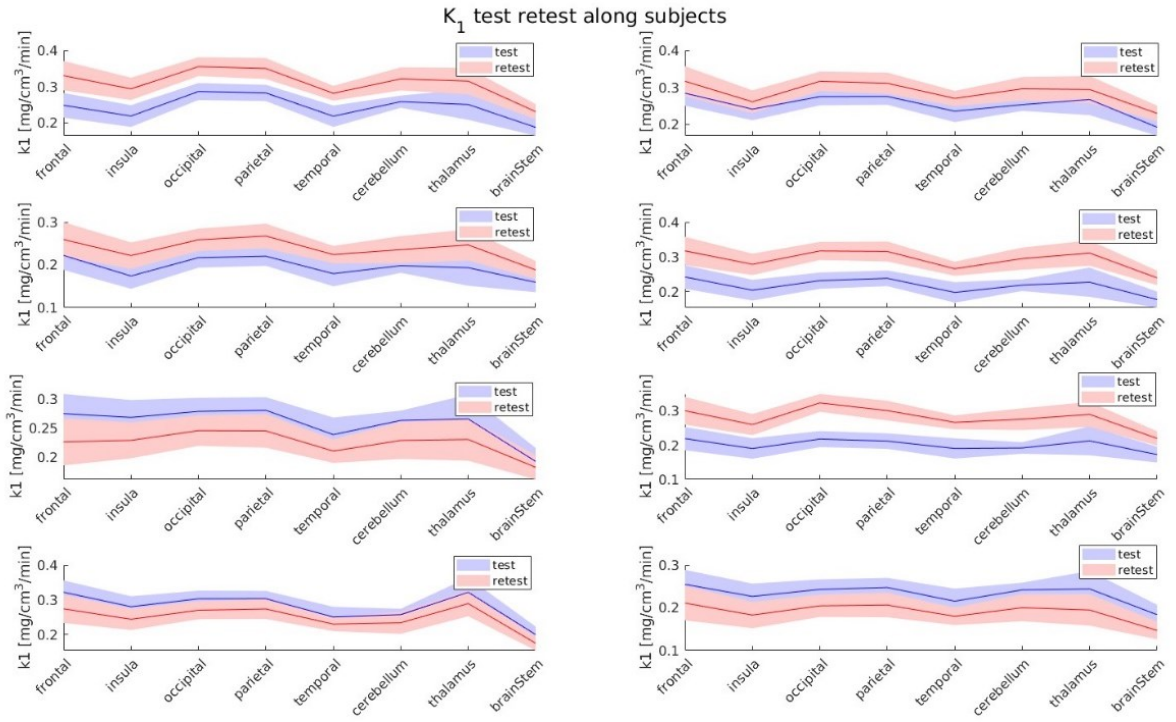

Figure 4.7. K1 estimates across ROIs in test and retest.

4.4 Regression model of K_1

A linear mixed-effects model was employed to analyse the K_1 estimates, taking into account various factors, such as subjects' age, genotype classification, gender, the ratio of the administered dose adjusted for weight (DW), and the body mass index (BMI). Notably, no significant correlation was identified between the physiological values and the mean K_1 across all regions of interest (ROIs) for each subject.

Subsequently, a linear mixed-effects model was applied to the K_1 estimates for each ROI, including both lobes and subcortical regions. In this analysis, significant positive correlations between dose-to-weight ratio (DW) and K_1 estimates were observed in the brain stem (Table 4.1).

	Age $(\boldsymbol{\beta}, \boldsymbol{p})$	**Gender** $(\boldsymbol{\beta}, \boldsymbol{p})$	**Genotype** $(\boldsymbol{\beta}, \boldsymbol{p})$	**DW** $(\boldsymbol{\beta}, \boldsymbol{p})$	**BMI** $(\boldsymbol{\beta}, \boldsymbol{p})$	$\boldsymbol{R^2}$
Frontal	-0.0004, p=0.20	0.003, p=0.84	0.01, p=0.26	0.01, p=0.40	-0.002, p=0.31	0.14
Insula	-0.0003, p=0.44	-0.002, p=0.89	0.011, p=0.34	0.01, p=0.50	-0.003, p=0.20	0.13
Occipital	-0.0005, p=0.20	0.041, p=0.73	0.011, p=0.36	0.02, p=0.12	-0.001, p=0.49	0.18
Parietal	-0.0004, p=0.45	-0.003, p=0.80	0.07, p=0.45	0.015, p=0.22	-0.002, p=0.32	0.19
Temporal	-0.0006, p=0.07	-0.002, p=0.85	0.01, p=0.31	0.01, p=0.31	-0.002, p=0.24	0.21
Cerebellum	-0.0004, p=0.18	-0.007, p=0.57	0.01, p=0.26	0.012, p=0.22	-0.002, p=0.32	0.19
Thalamus	-0.0003, p=0,47	0.004, p=0.74	0.015, p=0.21	0.02, p=0.20	-0.002, p=0.20	0.18
Brain Stem	-0.0004, p=0.12	-0.005, p=0.55	0.002, p=0.034	0.02, **p=0.03**	-0.0004, p=0.68	0.24

Table 4.1. Linear mixed-effects model: *describe the K1 (a parameter often associated with the rate of blood flow) in various brain lobes (frontal, insula, occipital, parietal, temporal) and subcortical regions (cerebellum, thalamus, brain stem).*

The stepwise regression analysis revealed significant positive correlations between the dose-to-weight ratio (DW) and K_1 estimates in the occipital and temporal lobes, as well as in the cerebellum and brain stem. Additionally, significant negative correlations were found between BMI and K_1 estimates in the frontal, insula, and parietal lobes, as well as in the thalamus (table 4.2).

	Age ($\boldsymbol{\beta}, \boldsymbol{p}$)	**Gender ($\boldsymbol{\beta}, \boldsymbol{p}$)**	**Genotype ($\boldsymbol{\beta}, \boldsymbol{p}$)**	**DW ($\boldsymbol{\beta}, \boldsymbol{p}$)**	**BMI ($\boldsymbol{\beta}, \boldsymbol{p}$)**	**$\boldsymbol{R^2}$**
Frontal	—	—	—	—	-0.004, **p=0.007**	0.10
Insula	—	—	—	—	-0.004, **p=0.002**	0.13
Occipital	—	—	—	0.029, **p=0.003**	—	0.12
Parietal	—	—	—	—	-0.004, **p=0.013**	0.080
Temporal	—	—	—	0.025, **p=0.002**	—	0.13
Cerebellum	—	—	—	0.028, **p=0.002**	—	0.14
Thalamus	—	—	—	—	-0.005, **p=0.002**	0.13
Brain Stem	—	—	—	0.027, **p<0.016**	—	0.21

Table 4.2. Step wise regression model*: describe the K1 (a parameter often associated with the rate of blood flow) in various brain lobes (frontal, insula, occipital, parietal, temporal) and subcortical regions (cerebellum, thalamus, brain stem).*

To note, in the linear mixed effect and step wire regression models, R^2 values range from 0.13 to 0.24 and from 0.080 to 0.21 respectively, which suggests that the independent variables collectively explain a modest to moderate proportion of the variance in K_1 estimates in the different brain regions.

The scatter plot in the Figure 4.8 illustrates the significant positive correlation between the mean 1T1K-C_p K_1 and the dose-to-weight ratio (DM) ($\rho = 0.35, p_{value} = 0.0032$), and the

significant negative correlation with the body mass index (BMI) ($\rho = -0.35, p_{value} = 0.0031$).

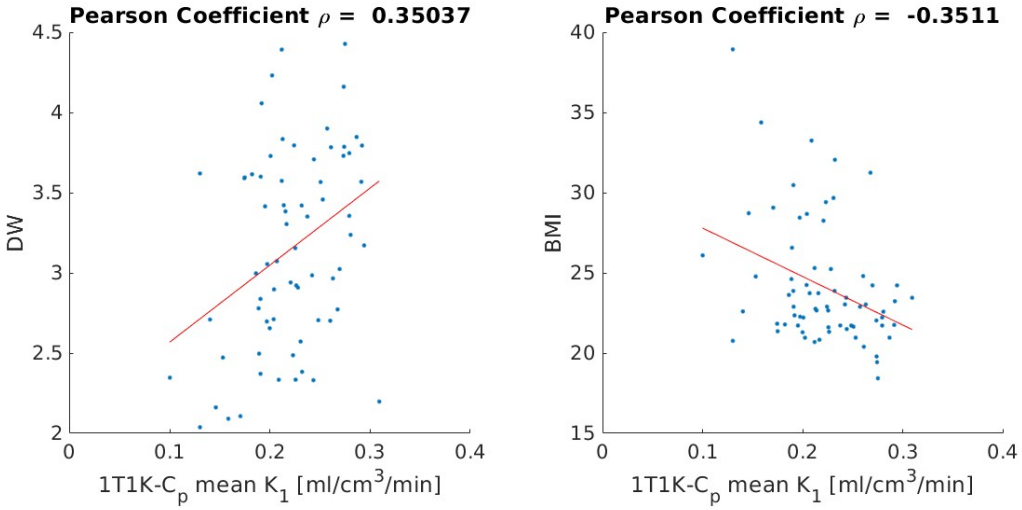

***Figure 4.8 illustrates two comparisons**: In the left panel, it showcases the comparison between the mean of 1T1K-Cp K1 and the dose-to-weight ratio (DW). On the right panel, it displays the comparison between the mean of 1T1K-Cp K1 and the body mass index (BMI).*

4.5 Comparison HC vs MS

4.5.1 Cerebral cortex

Between-subjects comparison shows significant differences in the K_1 estimate, derived from the cortex, between healthy controls and multiple sclerosis patients ($\rho < 0.001$). To note, the lowest K_1 estimate were found for the multiple sclerosis patients, and even if the K_1 estimate differ, the topological patter between the two groups is very similar (Figure 4.9 a).

Significant differences in the K1 estimates between healthy controls and each clinical subtype were found with a $\rho < 0.001$. Moreover, even if relapsing-remitting MS and secondary progressive MS has the closest K_1 estimates, are significantly different ($\rho = 0.001$). In contrast, primary progressive MS exhibited lower K_1 estimates, which are significantly different from both RRMS ($\rho < 0.001$) and SPMS ($\rho < 0.001$) (Figure 4.9 b).

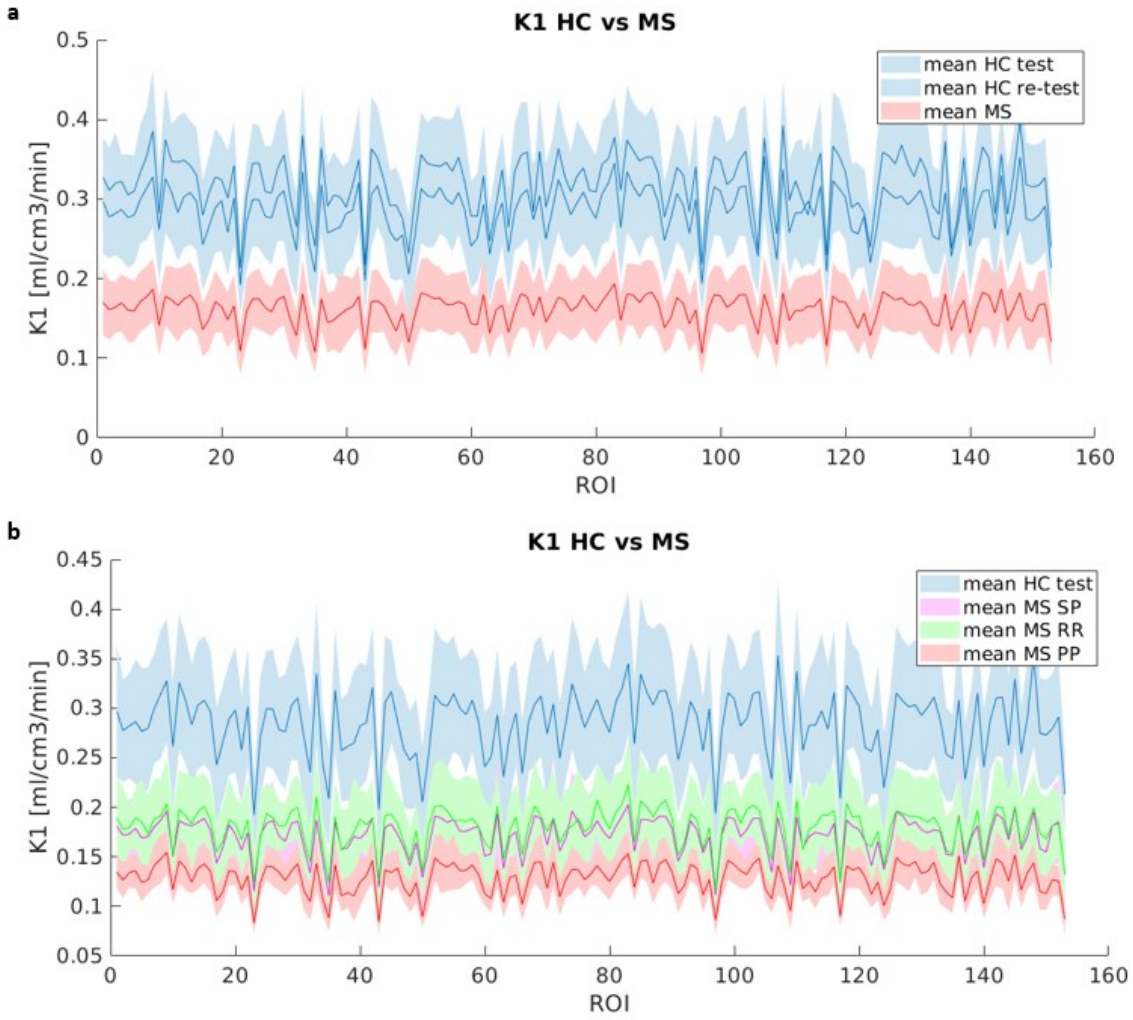

Figure 3.9 Between-subject comparison of K1 estimates in healthy controls and sclerosis multiple patients: *the panel a show the K1 estimates across patients in HC and MS patients. Meanwhile, the panel b shows the different clinical subtypes of MS patient in comparison to HC.*

4.5.2 White matter and normal appearing white matter

Intra-subject correlation of the K_1 estimate values, do not present significant differences ($\rho = 0.16$) between the white matter and normal-appearing white matter. In Figure 4.10 shows that, in almost all the patients, the K_1 estimate across ROIs of the lesions in the white matter tend to be higher than the ones in the normal-appearing white matter. Additionally, looking to the clinical subtypes, the K_1 estimate of the PPMS remain the lowest ones.

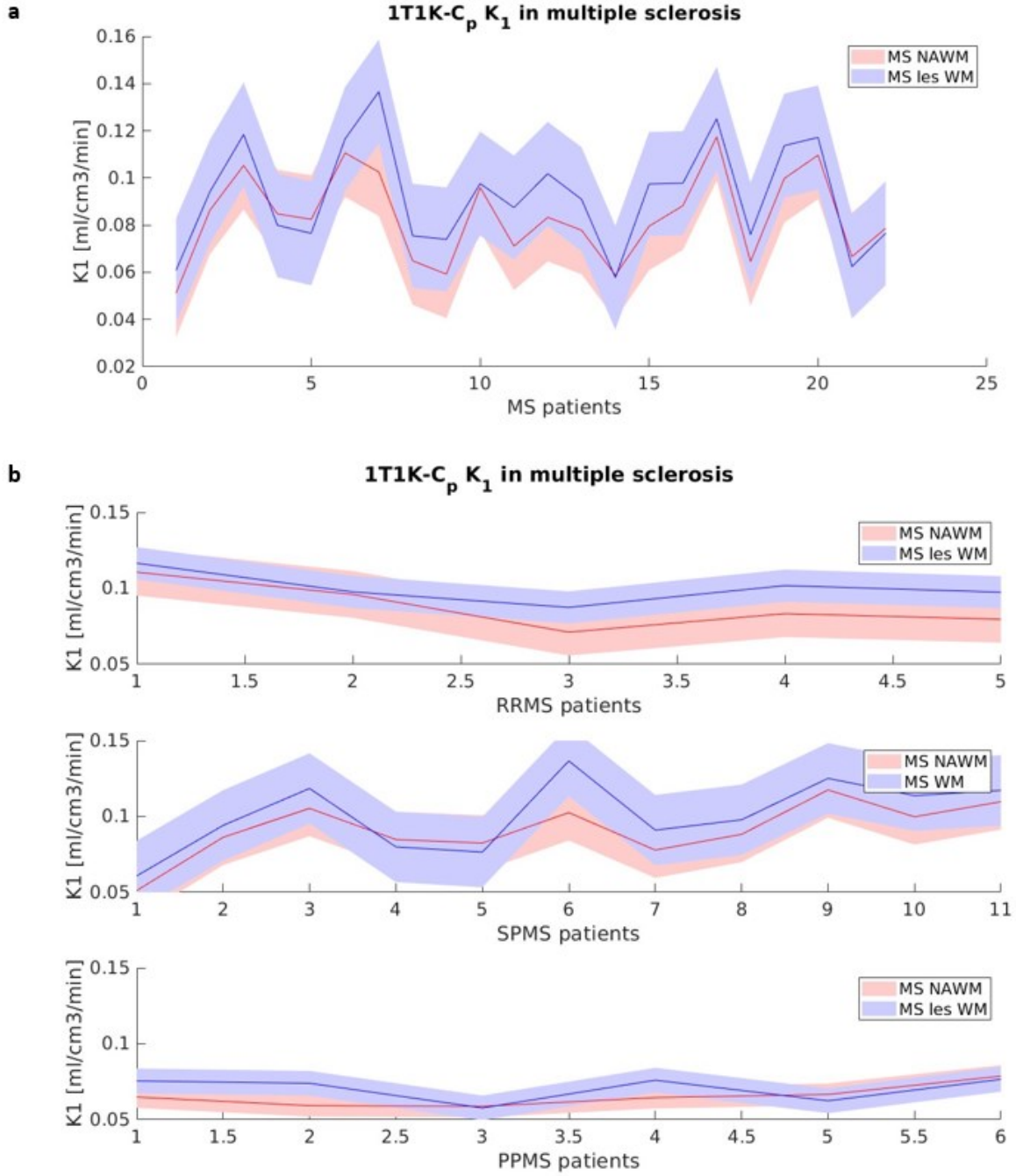

Figure 4.10 Intra-subject comparison of K_1 estimates in sclerosis multiple patients: *the panel a show the K_1 estimates across ROIs in normal-appearing white matter and in white matter lesions. Meanwhile, the panel b shows the different clinical subtypes of MS patient.*

Chapter 5 -

DISCUSSION

The method that was used in this thesis is a wholly non-invasive approach for quantifying K_1 and R_1 PET imaging parameters through fitting the early phase of the tracer dynamic.

The validation, achieved through comparison with the reference-standard blood-based estimates, revealed significant intra-subject and between-subjects correlations between the 2T4K-C_p and the 1T1K-IDIF K_1 estimates, using each of the three tested input functions. Conversely, when comparing 1T1K-C_p and 1T1K-C_b to 2T4K-C_p K_1 estimates, a reduced bias was reported. However, for the 1T1K-IDIF, a high and variable bias was noted, contingent on the IDIF variability to approximate blood input functions.

A good intra-subject correlation was observed for all comparisons between test-retest 1T1K-IDIF K_1 estimates. Across each subject, the physiological pattern of K_1 estimates remained consistent across the region of interest (ROIs). A low mean relative difference across all the ROIs was reported, but the high standard deviation indicates the variability or spread around this average difference, implying a significant amount of variation in the relative differences among the ROIs. This broad range of variation warrants further investigation and should be taken into consideration when interpreting the results.

The stepwise regression analysis and the linear mixed effect model unveiled significant positive correlations between the dose-to-weight ratio (DW) and K_1 estimates in the occipital and temporal lobes, as well as in the cerebellum and brain stem. Furthermore, it revealed significant negative correlations between BMI and K_1 estimates in the frontal, insula, and parietal lobes, as well as in the thalamus.

Given the comparable performances between 1T1K-C_p and 1T1K-C_b with the reference standard, the most challenging assumption for 1T1K-IDIF is the use of IDIF as a proxy for blood input (hypothesis 3), rather than the assumptions related to simplified modeling (hypothesis 1) or negligible metabolites (hypothesis 2). The bias effect associated with this assumption can be completely mitigated when attempting to estimate relative measures like R_1. In practice, the primary challenge in applying the method is indeed tied to the extraction of a reliable input function from the dynamic PET images of the tracer.

Another limitation of this study is associated with the selection of the time window for model fitting. The fit window was determined after conducting a sensitivity analysis and assessing metabolite production, taking into account factors such as the tracer's kinetics, tracer metabolism, and the temporal resolution of the dynamic PET scan. These considerations determined the total number of samples used for model fitting within a fixed fit time window. It's important to note that a longer window and higher temporal resolution lead to a greater number of samples, thereby improving the expected precision of the K_1 estimates and reducing the coefficient of variation.

For what concern the comparison between healthy controls and multiple sclerosis patients, the following consideration about the interpretability of the results have to be done.

The gadolinium enhancement observed in the initial three weeks of lesion formation is linked to the heightened permeability of the blood-brain barrier (BBB). This enhancement presents a challenge when studying specific variations in blood influx, as there is a leakage of intermediate molecules, complicating the isolation and precise analysis of changes in blood flow. Furthermore, to our knowledge, the relationship of these perfusion variations with the demyelination state within the white matter has never been investigated. The analysed influx rate constant K_1 (ml/cm^3/min), which signifies the rate of the tracer crossing the blood-brain barrier (BBB) from the plasma or blood compartment, emerges as a promising biomarker for detecting pathological processes in brain diseases. Its significance lies in its connection to cerebral blood flow (F, ml/cm^3/min) and the unidirectional extraction fraction (E) from blood into the brain during the tracer's initial pass through the capillary bed. However, distinguishing between these two values can be challenging, and for a more comprehensive understanding of K_1 estimates in multiple sclerosis further analysis have to be done.

The decreased K_1 estimates from the cerebral cortex in multiple sclerosis patients, in comparison to healthy controls, may be attributed to a widespread cerebral hypoperfusion observed in MS patients. This phenomenon seems to persist from the early stages to more advanced phases of the disease. It's worth noting that the cerebral cortex mask employed includes grey matter lesions. The gadolinium enhanced that is seen in the first three week of lesion formation is known to be due to the BBB increase of permeability and makes hard to specifically study the variation of blood influx, since there is a leakage of intermediate molecules. Cerebral blood flow imaging, such as dynamic susceptibility contrast (DSC), showed that the lesions in multiple sclerosis seems to be characterized by hypoperfusion. Is

interesting to note that imaging studies demonstrating hypoperfusion in patients with multiple sclerosis have revealed regional anatomical heterogeneities (Law et al., 2004). Notably, it has been demonstrated that transiently, approximately three weeks before the appearance of contrast enhancement (which serves as a reference for the radiological zero moment of lesion birth), transient hyper-perfusion could be observed in some pre-lesions (Wuerfel et al., 2004). This hyper-perfusion preceded the onset of hypoperfusion in the prelesion and subsequently in the established lesion.

In conclusion, this study gives valuable insights in the analysis of the blood-to-brain tracer exchange in [18F] DPA714 PET in multiple sclerosis patients. It is evident that further investigations are imperative to unravel the intricacies of this complex interplay. To advance our understanding, future analyses must focus on distinguishing between grey matter lesions and the cortex, as well as differentiating various lesions within both grey and white matter, particularly those without gadolinium enhancement. Moreover, adopting a voxel-wise approach will be paramount in unraveling the subtle nuances that may underlie these relationships. These proposed analyses not only stand as essential steps toward a comprehensive comprehension but also pave the way for a more nuanced understanding of the pathophysiological mechanisms at play in multiple sclerosis. By undertaking these future endeavors, we can hope to refine our knowledge and contribute meaningfully to the advancement of diagnostic and therapeutic.

CONCLUSIONS

The non-invasive method employed in this thesis for quantifying $K_{1,}$ and R_1 PET imaging parameters yielded promising results, especially in comparisons with blood-based estimates. The validation demonstrated significant correlations, with notable variations observed when using different input functions. Test-retest consistency was generally good, though variability across regions of interest warrants further exploration. Regression analysis revealed intriguing associations between dose-to-weight ratio (DW), BMI, and K_1 estimates in various brain regions.

The study highlighted the challenges associated with using an image-derived input function (IDIF) as a proxy for blood input, and the importance of the selection of the time window for model fitting.

A more comprehensive understanding of K_1 estimates in multiple sclerosis patients require a further analysis. Despite the insights gained, the study emphasizes the need for further investigations. These future endeavors aim to refine our understanding of the intricate interplay in multiple sclerosis, contributing to advancements in diagnostic and therapeutic approaches.

BIBLIOGRAPHY

Absinta, M., Lassmann, H., & Trapp, B. D. (2020). Mechanisms underlying progression in multiple sclerosis. In *Current Opinion in Neurology* (Vol. 33, Issue 3). https://doi.org/10.1097/WCO.0000000000000818

Albert, M., Antel, J., Brück, W., & Stadelmann, C. (2007). Extensive cortical remyelination in patients with chronic multiple sclerosis. *Brain Pathology*, *17*(2). https://doi.org/10.1111/j.1750-3639.2006.00043.x

Androdias, G., Reynolds, R., Chanal, M., Ritleng, C., Confavreux, C., & Nataf, S. (2010). Meningeal T cells associate with diffuse axonal loss in multiple sclerosis spinal cords. *Annals of Neurology*, *68*(4). https://doi.org/10.1002/ana.22054

Ascherio, A., Munger, K. L., White, R., Köchert, K., Simon, K. C., Polman, C. H., Freedman, M. S., Hartung, H. P., Miller, D. H., Montalbán, X., Edan, G., Barkhof, F., Pleimes, D., Radü, E. W., Sandbrink, R., Kappos, L., & Pohl, C. (2014). Vitamin D as an early predictor of multiple sclerosis activity and progression. *JAMA Neurology*, *71*(3). https://doi.org/10.1001/jamaneurol.2013.5993

Banati, R. B., Newcombe, J., Gunn, R. N., Cagnin, A., Turkheimer, F., Heppner, F., Price, G., Wegner, F., Giovannoni, G., Miller, D. H., Perkin, G. D., Smith, T., Hewson, A. K., Bydder, G., Kreutzberg, G. W., Jones, T., Cuzner, M. L., & Myers, R. (2000). The peripheral benzodiazepine binding site in the brain in multiple sclerosis. Quantitative in vivo imaging of microglia as a measure of disease activity. *Brain*, *123*(11). https://doi.org/10.1093/brain/123.11.2321

Bertoldo, A., Rizzo, G., & Veronese, M. (2014). Deriving physiological information from PET images: From SUV to compartmental modelling. In *Clinical and Translational Imaging* (Vol. 2, Issue 3). https://doi.org/10.1007/s40336-014-0067-x

Bevan, R. J., Evans, R., Griffiths, L., Watkins, L. M., Rees, M. I., Magliozzi, R., Allen, I., McDonnell, G., Kee, R., Naughton, M., Fitzgerald, D. C., Reynolds, R., Neal, J. W., & Howell, O. W. (2018). Meningeal inflammation and cortical demyelination in acute multiple sclerosis. *Annals of Neurology*, *84*(6). https://doi.org/10.1002/ana.25365

Bjornevik, K., Cortese, M., Healy, B. C., Kuhle, J., Mina, M. J., Leng, Y., Elledge, S. J., Niebuhr, D. W., Scher, A. I., Munger, K. L., & Ascherio, A. (2022). Longitudinal analysis reveals high prevalence of Epstein-Barr virus associated with multiple sclerosis. *Science*, *375*(6578). https://doi.org/10.1126/science.abj8222

Bodini, B., Tonietto, M., Airas, L., & Stankoff, B. (2021). Positron emission tomography in multiple sclerosis — straight to the target. *Nature Reviews Neurology*, *17*(11), 663–675. https://doi.org/10.1038/s41582-021-00537-1

Bonsack, F., Alleyne, C. H., & Sukumari-Ramesh, S. (2016). Augmented expression of TSPO after intracerebral hemorrhage: A role in inflammation? *Journal of Neuroinflammation*, *13*(1). https://doi.org/10.1186/s12974-016-0619-2

Borgström, M., Tisell, A., Link, H., Wilhelm, E., Lundberg, P., & Huang-Link, Y. (2020). Retinal thinning and brain atrophy in early MS and CIS. *Acta Neurologica Scandinavica*, *142*(5). https://doi.org/10.1111/ane.13282

Calabrese, M., Poretto, V., Favaretto, A., Alessio, S., Bernardi, V., Romualdi, C., Rinaldi, F., Perini, P., & Gallo, P. (2012). Cortical lesion load associates with progression of disability in multiple sclerosis. *Brain*, *135*(10). https://doi.org/10.1093/brain/aws246

Carswell, R. (1833). XX. Pathological Anatomy. Illustrations of the Elementary Forms of Disease. *The American Journal of the Medical Sciences*, *12*(24). https://doi.org/10.1097/00000441-183312240-00020

Cassan, C., & Liblau, R. S. (2007). Immune tolerance and control of CNS autoimmunity: From animal models to MS patients. In *Journal of Neurochemistry* (Vol. 100, Issue 4). https://doi.org/10.1111/j.1471-4159.2006.04270.x

Charbonneau, P., Syrota, A., Crouzel, C., Valois, J. M., & Prenant, C. (1986). Peripheral-type benzodiazepine receptors in the living heart characterized by positron emission tomography. *Circulation*, *73*(3). https://doi.org/10.1161/01.CIR.73.3.476

Charcot JM. (1868). Histologie de la sclérose en plaques. *Gazette Des Hopitaux*, *41*.

Chen, K., Bandy, D., Reiman, E., Huang, S. C., Lawson, M., Feng, D., Yun, L. S., & Palant, A. (1998). Noninvasive quantification of the cerebral metabolic rate for glucose using positron emission tomography, 18F-fluoro-2-deoxyglucose, the Patlak method, and an image-derived input function. *Journal of Cerebral Blood Flow and Metabolism*, *18*(7). https://doi.org/10.1097/00004647-199807000-00002

Choi, S. R., Howell, O. W., Carassiti, D., Magliozzi, R., Gveric, D., Muraro, P. A., Nicholas, R., Roncaroli, F., & Reynolds, R. (2012). Meningeal inflammation plays a role in the pathology of primary progressive multiple sclerosis. *Brain*, *135*(10). https://doi.org/10.1093/brain/aws189

Cobelli, C., Finkelstein, L., & Carson, E. R. (1982). Mathematical modelling of endocrine and metabolic systems: Model formulation, identification and validation. *Mathematics and Computers in Simulation*, *24*(6). https://doi.org/10.1016/0378-4754(82)90641-3

Cobelli, C., Foster, D., & Toffolo, G. (2002). Tracer Kinetics in Biomedical Research. In *Tracer Kinetics in Biomedical Research*. https://doi.org/10.1007/b112199

Cosenza-Nashat, M., Zhao, M. L., Suh, H. S., Morgan, J., Natividad, R., Morgello, S., & Lee, S. C. (2009). Expression of the translocator protein of 18 kDa by microglia, macrophages and astrocytes based on immunohistochemical localization in abnormal human brain. *Neuropathology and Applied Neurobiology*, *35*(3). https://doi.org/10.1111/j.1365-2990.2008.01006.x

Cramer, S. P., Simonsen, H., Frederiksen, J. L., Rostrup, E., & Larsson, H. B. W. (2014). Abnormal blood-brain barrier permeability in normal appearing white matter in multiple sclerosis investigated by MRI. *NeuroImage: Clinical*, *4*, 182–189. https://doi.org/10.1016/j.nicl.2013.12.001

Cree, B. A. C., Arnold, D. L., Chataway, J., Chitnis, T., Fox, R. J., Pozo Ramajo, A., Murphy, N., & Lassmann, H. (2021). Secondary Progressive Multiple Sclerosis: New Insights. In *Neurology* (Vol. 97, Issue 8). https://doi.org/10.1212/WNL.0000000000012323

Crone, C. (1963). The Permeability of Capillaries in Various Organs as Determined by Use of the 'Indicator Diffusion' Method. *Acta Physiologica Scandinavica*, *58*(4). https://doi.org/10.1111/j.1748-1716.1963.tb02652.x

Cruveilhier J. (1833). Art. XIII. Anatomie Pathologique du Corps Humain, ou Descriptions, avec Figures Lithographiées et Coloriées, des Diverses alterations Morbides dont le Corps Humain est susceptible. *The American Journal of the Medical Sciences*, *12*(24). https://doi.org/10.1097/00000441-183312240-00013

Datta, G., Colasanti, A., Rabiner, E. A., Gunn, R. N., Malik, O., Ciccarelli, O., Nicholas, R., Van Vlierberghe, E., Van Hecke, W., Searle, G., Santos-Ribeiro, A., & Matthews, P. M. (2017). Neuroinflammation and its relationship to changes in brain volume and white matter lesions in multiple sclerosis. *Brain*, *140*(11). https://doi.org/10.1093/brain/awx228

Dendrou, C. A., Fugger, L., & Friese, M. A. (2015). Immunopathology of multiple sclerosis. In *Nature Reviews Immunology* (Vol. 15, Issue 9, pp. 545–558). Nature Publishing Group. https://doi.org/10.1038/nri3871

D'Haeseleer, M., Hostenbach, S., Peeters, I., El Sankari, S., Nagels, G., De Keyser, J., & D'Hooghe, M. B. (2015). Cerebral hypoperfusion: A new pathophysiologic concept in multiple sclerosis? In *Journal of Cerebral Blood Flow and Metabolism* (Vol. 35, Issue 9). https://doi.org/10.1038/jcbfm.2015.131

Dodelet-Devillers, A., Cayrol, R., Van Horssen, J., Haqqani, A. S., De Vries, H. E., Engelhardt, B., Greenwood, J., & Prat, A. (2009). Functions of lipid raft membrane microdomains at the blood-brain barrier. In *Journal of Molecular Medicine* (Vol. 87, Issue 8). https://doi.org/10.1007/s00109-009-0488-6

Dupont, A. C., Largeau, B., Ribeiro, M. J. S., Guilloteau, D., Tronel, C., & Arlicot, N. (2017). Translocator protein-18 kDa (TSPO) positron emission tomography (PET) imaging and its clinical impact in neurodegenerative diseases. In *International Journal of Molecular Sciences* (Vol. 18, Issue 4). https://doi.org/10.3390/ijms18040785

Fan, Z., Harold, D., Pasqualetti, G., Williams, J., Brooks, D. J., & Edison, P. (2015). Can studies of neuroinflammation in a TSPO genetic subgroup (HAB or MAB) be applied to the entire AD cohort? *Journal of Nuclear Medicine*, *56*(5). https://doi.org/10.2967/jnumed.114.149443

Filippi, M., Bar-Or, A., Piehl, F., Preziosa, P., Solari, A., Vukusic, S., & Rocca, M. A. (2018). Multiple sclerosis. *Nature Reviews Disease Primers*, *4*(1). https://doi.org/10.1038/s41572-018-0041-4

Filippi, M., Brück, W., Chard, D., Fazekas, F., Geurts, J. J. G., Enzinger, C., Hametner, S., Kuhlmann, T., Preziosa, P., Rovira, À., Schmierer, K., Stadelmann, C., & Rocca, M. A. (2019). Association between pathological and MRI findings in multiple sclerosis. In *The Lancet Neurology* (Vol. 18, Issue 2). https://doi.org/10.1016/S1474-4422(18)30451-4

Filippi, M., Preziosa, P., & Rocca, M. A. (2014). Magnetic resonance outcome measures in multiple sclerosis trials: Time to rethink? In *Current Opinion in Neurology* (Vol. 27, Issue 3). https://doi.org/10.1097/WCO.0000000000000095

Frank, J. A., Stone, L. A., Smith, M. E., Albert, P. S., Maloni, H., & McFarland, H. F. (1994). Serial contrast-enhanced magnetic resonance imaging in patients with early relapsing-remitting multiple sclerosis: Implications for treatment trials. *Annals of Neurology*, *36*(SUPPL.). https://doi.org/10.1002/ana.410360719

Frischer, J. M., Bramow, S., Dal-Bianco, A., Lucchinetti, C. F., Rauschka, H., Schmidbauer, M., Laursen, H., Sorensen, P. S., & Lassmann, H. (2009). The relation between inflammation

and neurodegeneration in multiple sclerosis brains. *Brain*, *132*(5). https://doi.org/10.1093/brain/awp070

Frischer, J. M., Weigand, S. D., Guo, Y., Kale, N., Parisi, J. E., Pirko, I., Mandrekar, J., Bramow, S., Metz, I., Brück, W., Lassmann, H., & Lucchinetti, C. F. (2015). Clinical and pathological insights into the dynamic nature of the white matter multiple sclerosis plaque. *Annals of Neurology*, *78*(5). https://doi.org/10.1002/ana.24497

Frohman, E. M., Racke, M. K., & Raine, C. S. (2006). Multiple Sclerosis — The Plaque and Its Pathogenesis. *New England Journal of Medicine*, *354*(9). https://doi.org/10.1056/nejmra052130

Fung, E. K., Planeta-Wilson, B., Mulnix, T., & Carson, R. E. (2009). A multimodal approach to image-derived input functions for brain PET. *IEEE Nuclear Science Symposium Conference Record*. https://doi.org/10.1109/NSSMIC.2009.5401977

Gaitán, M. I., Shea, C. D., Evangelou, I. E., Stone, R. D., Fenton, K. M., Bielekova, B., Massacesi, L., & Reich, D. S. (2011). Evolution of the blood-brain barrier in newly forming multiple sclerosis lesions. *Annals of Neurology*, *70*(1). https://doi.org/10.1002/ana.22472

García-Lorenzo, D., Lavisse, S., Leroy, C., Wimberley, C., Bodini, B., Remy, P., Veronese, M., Turkheimer, F., Stankoff, B., & Bottlaender, M. (2018). Validation of an automatic reference region extraction for the quantification of [18 F]DPA-714 in dynamic brain PET studies. *Journal of Cerebral Blood Flow and Metabolism*, *38*(2). https://doi.org/10.1177/0271678X17692599

Ge, Y., Law, M., Johnson, G., Herbert, J., Babb, J. S., Mannon, L. J., & Grossman, R. I. (2005). Dynamic susceptibility contrast perfusion MR imaging of multiple sclerosis lesions: Characterizing hemodynamic impairment and inflammatory activity. *American Journal of Neuroradiology*, *26*(6).

Gershen, L. D., Zanotti-Fregonara, P., Dustin, I. H., Liow, J. S., Hirvonen, J., Kreisl, W. C., Jenko, K. J., Inati, S. K., Fujita, M., Morse, C. L., Brouwer, C., Hong, J. S., Pike, V. W., Zoghbi, S. S., Innis, R. B., & Theodore, W. H. (2015). Neuroinflammation in temporal lobe epilepsy measured using positron emission tomographic imaging of translocator protein. *JAMA Neurology*, *72*(8). https://doi.org/10.1001/jamaneurol.2015.0941

Giannetti, P., Politis, M., Su, P., Turkheimer, F. E., Malik, O., Keihaninejad, S., Wu, K., Waldman, A., Reynolds, R., Nicholas, R., & Piccini, P. (2015). Increased PK11195-PET binding in normal-appearing white matter in clinically isolated syndrome. *Brain : A Journal of Neurology*, *138*. https://doi.org/10.1093/brain/awu331

Gilmore, C. P., Donaldson, I., Bö, L., Owens, T., Lowe, J., & Evangelou, N. (2009). Regional variations in the extent and pattern of grey matter demyelination in multiple sclerosis: A comparison between the cerebral cortex, cerebellar cortex, deep grey matter nuclei and the spinal cord. *Journal of Neurology, Neurosurgery and Psychiatry*, *80*(2). https://doi.org/10.1136/jnnp.2008.148767

Glass, C. K., Saijo, K., Winner, B., Marchetto, M. C., & Gage, F. H. (2010). Mechanisms Underlying Inflammation in Neurodegeneration. In *Cell* (Vol. 140, Issue 6). https://doi.org/10.1016/j.cell.2010.02.016

Greer, J. M., & McCombe, P. A. (2011). Role of gender in multiple sclerosis: Clinical effects and potential molecular mechanisms. In *Journal of Neuroimmunology* (Vol. 234, Issues 1–2). https://doi.org/10.1016/j.jneuroim.2011.03.003

Hagens, M. H. J., Golla, S. V., Wijburg, M. T., Yaqub, M., Heijtel, D., Steenwijk, M. D., Schober, P., Brevé, J. J. P., Schuit, R. C., Reekie, T. A., Kassiou, M., Van Dam, A. M., Windhorst, A. D., Killestein, J., Barkhof, F., Van Berckel, B. N. M., & Lammertsma, A. A. (2018). In vivo assessment of neuroinflammation in progressive multiple sclerosis: A proof of concept study with [18F]DPA714 PET. *Journal of Neuroinflammation*, *15*(1). https://doi.org/10.1186/s12974-018-1352-9

Haider, L., Simeonidou, C., Steinberger, G., Hametner, S., Grigoriadis, N., Deretzi, G., Kovacs, G. G., Kutzelnigg, A., Lassmann, H., & Frischer, J. M. (2014). Multiple sclerosis deep grey matter: The relation between demyelination, neurodegeneration, inflammation and iron. *Journal of Neurology, Neurosurgery and Psychiatry*, *85*(12). https://doi.org/10.1136/jnnp-2014-307712

Haider, L., Zrzavy, T., Hametner, S., Höftberger, R., Bagnato, F., Grabner, G., Trattnig, S., Pfeifenbring, S., Brück, W., & Lassmann, H. (2016). The topograpy of demyelination and neurodegeneration in the multiple sclerosis brain. *Brain*, *139*(3). https://doi.org/10.1093/brain/awv398

Halder, S. K., & Milner, R. (2021). Hypoxia in multiple sclerosis; Is it the chicken or the egg? *Brain*, *144*(2). https://doi.org/10.1093/brain/awaa427

Hauser, S. L., & Cree, B. A. C. (2020). Treatment of Multiple Sclerosis: A Review. In *American Journal of Medicine* (Vol. 133, Issue 12). https://doi.org/10.1016/j.amjmed.2020.05.049

Hooker, J. M., & Carson, R. E. (2019). Human Positron Emission Tomography Neuroimaging. In *Annual Review of Biomedical Engineering* (Vol. 21). https://doi.org/10.1146/annurev-bioeng-062117-121056

Howell, O. W., Reeves, C. A., Nicholas, R., Carassiti, D., Radotra, B., Gentleman, S. M., Serafini, B., Aloisi, F., Roncaroli, F., Magliozzi, R., & Reynolds, R. (2011). Meningeal inflammation is widespread and linked to cortical pathology in multiple sclerosis. *Brain*, *134*(9). https://doi.org/10.1093/brain/awr182

Huang, H., Zhu, H., Xie, Q., Tian, X., Yang, X., Feng, F., Jiang, Q., Sheng, X., & Yang, Z. (2020). Evaluation of 124I-JS001 for hPD1 immuno-PET imaging using sarcoma cell homografts in humanized mice. *Acta Pharmaceutica Sinica B*, *10*(7). https://doi.org/10.1016/j.apsb.2020.02.004

Jain, P., Chaney, A. M., Carlson, M. L., Jackson, I. M., Rao, A., & James, M. L. (2020). Neuroinflammation pet imaging: Current opinion and future directions. *Journal of Nuclear Medicine*, *61*(8). https://doi.org/10.2967/jnumed.119.229443

Jersild, C., Svejgaard, A., & Fog, T. (1972). HL-A ANTIGENS AND MULTIPLE SCLEROSIS. In *The Lancet* (Vol. 299, Issue 7762). https://doi.org/10.1016/S0140-6736(72)90962-2

Juurlink, B. H. J. (2013). The Evidence for Hypoperfusion as a Factor in Multiple Sclerosis Lesion Development. *Multiple Sclerosis International*, *2013*. https://doi.org/10.1155/2013/598093

Kawachi, I., & Lassmann, H. (2017). Neurodegeneration in multiple sclerosis and neuromyelitis optica. In *Journal of Neurology, Neurosurgery and Psychiatry* (Vol. 88, Issue 2). https://doi.org/10.1136/jnnp-2016-313300

Klaver, R., De Vries, H. E., Schenk, G. J., & Geurts, J. J. G. (2013). Grey matter damage in multiple sclerosis A pathology perspective. *Prion*, *7*(1). https://doi.org/10.4161/pri.23499

Knezevic, D., & Mizrahi, R. (2018). Molecular imaging of neuroinflammation in Alzheimer's disease and mild cognitive impairment. In *Progress in Neuro-Psychopharmacology and Biological Psychiatry* (Vol. 80, pp. 123–131). Elsevier Inc. https://doi.org/10.1016/j.pnpbp.2017.05.007

Kreisl, W. C., Jenko, K. J., Hines, C. S., Hyoung Lyoo, C., Corona, W., Morse, C. L., Zoghbi, S. S., Hyde, T., Kleinman, J. E., Pike, V. W., McMahon, F. J., & Innis, R. B. (2013). A genetic polymorphism for translocator protein 18 kDa affects both in vitro and in vivo radioligand binding in human brain to this putative biomarker of neuroinflammation. *Journal of Cerebral Blood Flow and Metabolism*, *33*(1). https://doi.org/10.1038/jcbfm.2012.131

Krieger, S. C., Cook, K., de Nino, S., & Fletcher, M. (2016). The topographical model of multiple sclerosis: A dynamic visualization of disease course. *Neurology: Neuroimmunology and NeuroInflammation*, *3*(5). https://doi.org/10.1212/NXI.0000000000000279

Kuhnast, B., Damont, A., Hinnen, F., Catarina, T., Demphel, S., Le Helleix, S., Coulon, C., Goutal, S., Gervais, P., & Dollé, F. (2012). [18F]DPA-714, [18F]PBR111 and [18F]FEDAA1106-Selective radioligands for imaging TSPO 18kDa with PET: Automated radiosynthesis on a TRACERLAb FX-FN synthesizer and quality controls. *Applied Radiation and Isotopes*, *70*(3), 489–497. https://doi.org/10.1016/j.apradiso.2011.10.015

Kutzelnigg, A., Faber-Rod, J. C., Bauer, J., Lucchinetti, C. F., Sorensen, P. S., Laursen, H., Stadelmann, C., Brück, W., Rauschka, H., Schmidbauer, M., & Lassmann, H. (2007). Widespread demyelination in the cerebellar cortex in multiple sclerosis. *Brain Pathology*, *17*(1). https://doi.org/10.1111/j.1750-3639.2006.00041.x

Kutzelnigg, A., Lucchinetti, C. F., Stadelmann, C., Brück, W., Rauschka, H., Bergmann, M., Schmidbauer, M., Parisi, J. E., & Lassmann, H. (2005). Cortical demyelination and diffuse white matter injury in multiple sclerosis. *Brain*, *128*(11). https://doi.org/10.1093/brain/awh641

Larcher, J. C., Vayssiere, J. L., Le Marquer, F. J., Cordeau, L. R., Keane, P. E., Bachy, A., Gross, F., & Croizat, B. P. (1989). Effects of peripheral benzodiazepines upon the O2 consumption of neuroblastoma cells. *European Journal of Pharmacology*, *161*(2–3). https://doi.org/10.1016/0014-2999(89)90843-1

Lassmann, H. (2018). Multiple sclerosis pathology. In *Cold Spring Harbor Perspectives in Medicine* (Vol. 8, Issue 3). Cold Spring Harbor Laboratory Press. https://doi.org/10.1101/cshperspect.a028936

Lassmann, H., Van Horssen, J., & Mahad, D. (2012). Progressive multiple sclerosis: Pathology and pathogenesis. In *Nature Reviews Neurology* (Vol. 8, Issue 11). https://doi.org/10.1038/nrneurol.2012.168

Lavisse, S., García-Lorenzo, D., Peyronneau, M. A., Bodini, B., Thiriez, C., Kuhnast, B., Comtat, C., Remy, P., Stankoff, B., & Bottlaender, M. (2015). Optimized quantification of translocator protein radioligand 18F-DPA-714 uptake in the brain of genotyped healthy volunteers. *Journal of Nuclear Medicine*, *56*(7). https://doi.org/10.2967/jnumed.115.156083

Lavisse, S., Guillermier, M., Hérard, A. S., Petit, F., Delahaye, M., Van Camp, N. V., Haim, L. Ben, Lebon, V., Remy, P., Dollé, F., Delzescaux, T., Bonvento, G., Hantraye, P., & Escartin,

C. (2012). Reactive astrocytes overexpress TSPO and are detected by TSPO positron emission tomography imaging. *Journal of Neuroscience*, *32*(32). https://doi.org/10.1523/JNEUROSCI.1487-12.2012

Law, M., Saindane, A. M., Ge, Y., Babb, J. S., Johnson, G., Mannon, L. J., Herbert, J., & Grossman, R. I. (2004). Microvascular abnormality in relapsing-remitting multiple sclerosis: Perfusion MR imaging findings in normal-appearing white matter. *Radiology*, *231*(3). https://doi.org/10.1148/radiol.2313030996

Lazzarotto, A., Margoni, M., Franciotta, S., Zywicki, S., Riccardi, A., Poggiali, D., Anglani, M., & Gallo, P. (2020). Selective Cerebellar Atrophy Associates with Depression and Fatigue in the Early Phases of Relapse-Onset Multiple Sclerosis. *Cerebellum*, *19*(2). https://doi.org/10.1007/s12311-019-01096-4

Lee, N. J., Ha, S. K., Sati, P., Absinta, M., Luciano, N. J., Lefeuvre, J. A., Schindler, M. K., Leibovitch, E. C., Ryu, J. K., Petersen, M. A., Silva, A. C., Jacobson, S., Akassoglou, K., & Reich, D. S. (2018). Spatiotemporal distribution of fibrinogen in marmoset and human inflammatory demyelination. *Brain*, *141*(6). https://doi.org/10.1093/brain/awy082

Leonelli, E., Yague, J. G., Ballabio, M., Azcoitia, I., Magnaghi, V., Schumacher, M., Garcia-Segura, L. M., & Melcangi, R. C. (2005). Ro5-4864, a synthetic ligand of peripheral benzodiazepine receptor, reduces aging-associated myelin degeneration in the sciatic nerve of male rats. *Mechanisms of Ageing and Development*, *126*(11). https://doi.org/10.1016/j.mad.2005.06.001

Lin, D., Chang, Y. J., Strauss, J. F., & Miller, W. L. (1993). The human peripheral renzodiazepine receptor gene: Cloning and characterization of alternative splicing in normal tissues and in a patient with congenital lipoid adrenal hyperplasia. *Genomics*, *18*(3). https://doi.org/10.1016/S0888-7543(05)80367-2

Lin, Y., Pan, Y., Wang, M., Huang, X., Yin, Y., Wang, Y., Jia, F., Xiong, W., Zhang, N., & Jiang, J. Y. (2012). Bloodbrain barrier permeability is positively correlated with cerebral microvascular perfusion in the early fluid percussion-injured brain of the rat. *Laboratory Investigation*, *92*(11). https://doi.org/10.1038/labinvest.2012.118

Liptrot, M., Adams, K. H., Martiny, L., Pinborg, L. H., Lonsdale, M. N., Olsen, N. V., Holm, S., Svarer, C., & Knudsen, G. M. (2004). Cluster analysis in kinetic modelling of the brain: A noninvasive alternative to arterial sampling. *NeuroImage*, *21*(2). https://doi.org/10.1016/j.neuroimage.2003.09.058

Litton, J. E. (1997). Input function in PET brain studies using MR-defined arteries. In *Journal of Computer Assisted Tomography* (Vol. 21, Issue 6). https://doi.org/10.1097/00004728-199711000-00012

Lublin, F. D., Reingold, S. C., Cohen, J. A., Cutter, G. R., Sørensen, P. S., Thompson, A. J., Wolinsky, J. S., Balcer, L. J., Banwell, B., Barkhof, F., Bebo, B., Calabresi, P. A., Clanet, M., Comi, G., Fox, R. J., Freedman, M. S., Goodman, A. D., Inglese, M., Kappos, L., … Polman, C. H. (2014). Defining the clinical course of multiple sclerosis: The 2013 revisions. In *Neurology* (Vol. 83, Issue 3). https://doi.org/10.1212/WNL.0000000000000560

Lucchinetti, C., Brück, W., Parisi, J., Scheithauer, B., Rodriguez, M., & Lassmann, H. (2000). Heterogeneity of multiple sclerosis lesions: Implications for the pathogenesis of demyelination. *Annals of Neurology*, *47*(6). https://doi.org/10.1002/1531-8249(200006)47:6<707::AID-ANA3>3.0.CO;2-Q

Lucchinetti, C. F., Popescu, B. F. G., Bunyan, R. F., Moll, N. M., Roemer, S. F., Lassmann, H., Brück, W., Parisi, J. E., Scheithauer, B. W., Giannini, C., Weigand, S. D., Mandrekar, J., & Ransohoff, R. M. (2011). Inflammatory Cortical Demyelination in Early Multiple Sclerosis. *New England Journal of Medicine*, *365*(23). https://doi.org/10.1056/nejmoa1100648

Luchetti, S., Fransen, N. L., van Eden, C. G., Ramaglia, V., Mason, M., & Huitinga, I. (2018). Progressive multiple sclerosis patients show substantial lesion activity that correlates with clinical disease severity and sex: a retrospective autopsy cohort analysis. *Acta Neuropathologica*, *135*(4). https://doi.org/10.1007/s00401-018-1818-y

M. Filippi, P. Preziosa, M. Copetti, G. Riccitelli, M.A. Horsfield, V. Martinelli, G. Comi, & M.A. Rocca. (2013). Gray matter damage predicts the accumulation of disability 13 years later in MS. In *Neurology* (Vol. 81, Issue 20).

Machado-Santos, J., Saji, E., Tröscher, A. R., Paunovic, M., Liblau, R., Gabriely, G., Bien, C. G., Bauer, J., & Lassmann, H. (2018). The compartmentalized inflammatory response in the multiple sclerosis brain is composed of tissue-resident CD8+ T lymphocytes and B cells. *Brain*, *141*(7). https://doi.org/10.1093/brain/awy151

Magliozzi, R., Howell, O., Vora, A., Serafini, B., Nicholas, R., Puopolo, M., Reynolds, R., & Aloisi, F. (2007). Meningeal B-cell follicles in secondary progressive multiple sclerosis associate with early onset of disease and severe cortical pathology. *Brain*, *130*(4). https://doi.org/10.1093/brain/awm038

Magliozzi, R., Howell, O. W., Nicholas, R., Cruciani, C., Castellaro, M., Romualdi, C., Rossi, S., Pitteri, M., Benedetti, M. D., Gajofatto, A., Pizzini, F. B., Montemezzi, S., Rasia, S., Capra, R., Bertoldo, A., Facchiano, F., Monaco, S., Reynolds, R., & Calabrese, M. (2018). Inflammatory intrathecal profiles and cortical damage in multiple sclerosis. *Annals of Neurology*, *83*(4). https://doi.org/10.1002/ana.25197

Magliozzi, R., Howell, O. W., Reeves, C., Roncaroli, F., Nicholas, R., Serafini, B., Aloisi, F., & Reynolds, R. (2010). A Gradient of neuronal loss and meningeal inflammation in multiple sclerosis. *Annals of Neurology*, *68*(4). https://doi.org/10.1002/ana.22230

Magliozzi, R., Reynolds, R., & Calabrese, M. (2018). MRI of cortical lesions and its use in studying their role in MS pathogenesis and disease course. *Brain Pathology*, *28*(5). https://doi.org/10.1111/bpa.12642

Mahad, D. H., Trapp, B. D., & Lassmann, H. (2015). Pathological mechanisms in progressive multiple sclerosis. In *The Lancet Neurology* (Vol. 14, Issue 2). https://doi.org/10.1016/S1474-4422(14)70256-X

Margoni, M., Poggiali, D., Zywicki, S., Rubin, M., Lazzarotto, A., Franciotta, S., Anglani, M. G., Causin, F., Rinaldi, F., Perini, P., Filippi, M., & Gallo, P. (2021). Early red nucleus atrophy in relapse-onset multiple sclerosis. *Human Brain Mapping*, *42*(1). https://doi.org/10.1002/hbm.25213

McGinley, M., & Ontaneda, D. (2019). MS progression is predominantly driven by age-related mechanisms – NO. *Multiple Sclerosis Journal*, *25*(7). https://doi.org/10.1177/1352458518819712

Miller, D. H., & Leary, S. M. (2007). Primary-progressive multiple sclerosis. In *Lancet Neurology* (Vol. 6, Issue 10). https://doi.org/10.1016/S1474-4422(07)70243-0

Minagar, A., & Alexander, J. S. (2003). Blood-brain barrier disruption in multiple sclerosis. In *Multiple Sclerosis* (Vol. 9, Issue 6). https://doi.org/10.1191/1352458503ms965oa

Misra, A., Ganesh, S., Shahiwala, A., & Shah, S. P. (2003). Drug delivery to the central nervous system: A review. In *Journal of Pharmacy and Pharmaceutical Sciences* (Vol. 6, Issue 2).

Montalban, X., Arnold, D. L., Weber, M. S., Staikov, I., Piasecka-Stryczynska, K., Willmer, J., Martin, E. C., Dangond, F., Syed, S., & Wolinsky, J. S. (2019). Placebo-Controlled Trial of an Oral BTK Inhibitor in Multiple Sclerosis. *New England Journal of Medicine*, *380*(25). https://doi.org/10.1056/nejmoa1901981

Münzel, E. J., & Williams, A. (2013). Promoting remyelination in multiple sclerosis-recent advances. In *Drugs* (Vol. 73, Issue 18). https://doi.org/10.1007/s40265-013-0146-8

Nair, A., Frederick, T. J., & Miller, S. D. (2008). Astrocytes in multiple sclerosis: A product of their environment. In *Cellular and Molecular Life Sciences* (Vol. 65, Issue 17). https://doi.org/10.1007/s00018-008-8059-5

Nutma, E., Gebro, E., Marzin, M. C., van der Valk, P., Matthews, P. M., Owen, D. R., & Amor, S. (2021). Activated microglia do not increase 18 kDa translocator protein (TSPO) expression in the multiple sclerosis brain. *GLIA*, *69*(10). https://doi.org/10.1002/glia.24052

Nutma, E., Stephenson, J. A., Gorter, R. P., De Bruin, J., Boucherie, D. M., Donat, C. K., Breur, M., Van Der Valk, P., Matthews, P. M., Owen, D. R., & Amor, S. (2019). A quantitative neuropathological assessment of translocator protein expression in multiple sclerosis. *Brain*, *142*(11). https://doi.org/10.1093/brain/awz287

Odoardi, F., Sie, C., Streyl, K., Ulaganathan, V. K., Schläger, C., Lodygin, D., Heckelsmiller, K., Nietfeld, W., Ellwart, J., Klinkert, W. E. F., Lottaz, C., Nosov, M., Brinkmann, V., Spang, R., Lehrach, H., Vingron, M., Wekerle, H., Flügel-Koch, C., & Flügel, A. (2012). T cells become licensed in the lung to enter the central nervous system. *Nature*, *488*(7413). https://doi.org/10.1038/nature11337

Olsson, T., Barcellos, L. F., & Alfredsson, L. (2016). Interactions between genetic, lifestyle and environmental risk factors for multiple sclerosis. In *Nature Reviews Neurology* (Vol. 13, Issue 1). https://doi.org/10.1038/nrneurol.2016.187

Ontaneda, D., Fox, R. J., & Chataway, J. (2015). Clinical trials in progressive multiple sclerosis: Lessons learned and future perspectives. In *The Lancet Neurology* (Vol. 14, Issue 2). https://doi.org/10.1016/S1474-4422(14)70264-9

Ortiz, G. G., Pacheco-Moisés, F. P., Macías-Islas, M. Á., Flores-Alvarado, L. J., Mireles-Ramírez, M. A., González-Renovato, E. D., Hernández-Navarro, V. E., Sánchez-López, A. L., & Alatorre-Jiménez, M. A. (2014). Role of the Blood-Brain Barrier in Multiple Sclerosis. In *Archives of Medical Research* (Vol. 45, Issue 8). https://doi.org/10.1016/j.arcmed.2014.11.013

Owen, D. R., Narayan, N., Wells, L., Healy, L., Smyth, E., Rabiner, E. A., Galloway, D., Williams, J. B., Lehr, J., Mandhair, H., Peferoen, L. A. N., Taylor, P. C., Amor, S., Antel, J. P., Matthews, P. M., & Moore, C. S. (2017). Pro-inflammatory activation of primary microglia and macrophages increases 18 kDa translocator protein expression in rodents but not humans. *Journal of Cerebral Blood Flow and Metabolism*, *37*(8). https://doi.org/10.1177/0271678X17710182

Owen, D. R., Yeo, A. J., Gunn, R. N., Song, K., Wadsworth, G., Lewis, A., Rhodes, C., Pulford, D. J., Bennacef, I., Parker, C. A., Stjean, P. L., Cardon, L. R., Mooser, V. E., Matthews, P. M., Rabiner, E. A., & Rubio, J. P. (2012). An 18-kDa Translocator Protein (TSPO) polymorphism explains differences in binding affinity of the PET radioligand PBR28. *Journal of Cerebral Blood Flow and Metabolism*, *32*(1). https://doi.org/10.1038/jcbfm.2011.147

Papadopoulos, V., Lecanu, L., Brown, R. C., Han, Z., & Yao, Z. X. (2006). Peripheral-type benzodiazepine receptor in neurosteroid biosynthesis, neuropathology and neurological disorders. *Neuroscience*, *138*(3). https://doi.org/10.1016/j.neuroscience.2005.05.063

Patsopoulos, N. A., Barcellos, L. F., Hintzen, R. Q., Schaefer, C., van Duijn, C. M., Noble, J. A., Raj, T., Gourraud, P. A., Stranger, B. E., Oksenberg, J., Olsson, T., Taylor, B. V., Sawcer, S., Hafler, D. A., Carrington, M., De Jager, P. L., de Bakker, P. I. W., Bernardinelli, L., Booth, D., … Kermode, A. G. (2013). Fine-Mapping the Genetic Association of the Major Histocompatibility Complex in Multiple Sclerosis: HLA and Non-HLA Effects. *PLoS Genetics*, *9*(11). https://doi.org/10.1371/journal.pgen.1003926

Peruzzo, D., Castellaro, M., Calabrese, M., Veronese, E., Rinaldi, F., Bernardi, V., Favaretto, A., Gallo, P., & Bertoldo, A. (2013). Heterogeneity of cortical lesions in multiple sclerosis: An MRI perfusion study. *Journal of Cerebral Blood Flow and Metabolism*, *33*(3). https://doi.org/10.1038/jcbfm.2012.192

Petersen, M. A., Ryu, J. K., Chang, K. J., Etxeberria, A., Bardehle, S., Mendiola, A. S., Kamau-Devers, W., Fancy, S. P. J., Thor, A., Bushong, E. A., Baeza-Raja, B., Syme, C. A., Wu, M. D., Rios Coronado, P. E., Meyer-Franke, A., Yahn, S., Pous, L., Lee, J. K., Schachtrup, C., … Akassoglou, K. (2017). Fibrinogen Activates BMP Signaling in Oligodendrocyte Progenitor Cells and Inhibits Remyelination after Vascular Damage. *Neuron*, *96*(5). https://doi.org/10.1016/j.neuron.2017.10.008

Peterson, J. W., Bö, L., Mörk, S., Chang, A., & Trapp, B. D. (2001). Transected neurites, apoptotic neurons, and reduced inflammation in cortical multiple sclerosis lesions. *Annals of Neurology*, *50*(3). https://doi.org/10.1002/ana.1123

Petrova, N., Carassiti, D., Altmann, D. R., Baker, D., & Schmierer, K. (2018). Axonal loss in the multiple sclerosis spinal cord revisited. *Brain Pathology*, *28*(3). https://doi.org/10.1111/bpa.12516

Politis, M., Giannetti, P., Su, P., Turkheimer, F., Keihaninejad, S., Wu, K., Waldman, A., Malik, O., Matthews, P. M., Reynolds, R., Nicholas, R., & Piccini, P. (2012). Increased PK11195 PET binding in the cortex of patients with MS correlates with disability. *Neurology*, *79*(6). https://doi.org/10.1212/WNL.0b013e3182635645

Prineas, J. W., Kwon, E. E., Cho, E. S., Sharer, L. R., Barnett, M. H., Oleszak, E. L., Hoffman, B., & Morgan, B. P. (2001). Immunopathology of secondary-progressive multiple sclerosis. *Annals of Neurology*, *50*(5). https://doi.org/10.1002/ana.1255

Pulagam, K. R., Colás, L., Padro, D., Plaza-García, S., Gómez-Vallejo, V., Higuchi, M., Llop, J., & Martín, A. (2017). Evaluation of the novel TSPO radiotracer [18F] VUIIS1008 in a preclinical model of cerebral ischemia in rats. *EJNMMI Research*, *7*. https://doi.org/10.1186/s13550-017-0343-7

Ramanujam, R., Hedström, A. K., Manouchehrinia, A., Alfredsson, L., Olsson, T., Bottai, M., & Hillert, J. (2015). Effect of smoking cessation on multiple sclerosis prognosis. *JAMA Neurology*, *72*(10). https://doi.org/10.1001/jamaneurol.2015.1788

Renkin E. M. (1959). Transport of potassium-42 from blood to tissue in isolated mammalian skeletal muscles. *The American Journal of Physiology*, *197*. https://doi.org/10.1152/ajplegacy.1959.197.6.1205

Rissanen, E., Tuisku, J., Rokka, J., Paavilainen, T., Parkkola, R., Rinne, J. O., & Airas, L. (2014). In vivo detection of diffuse inflammation in secondary progressive multiple sclerosis using PET imaging and the radioligand11C-PK11195. *Journal of Nuclear Medicine*, *55*(6). https://doi.org/10.2967/jnumed.113.131698

Rocca, M. A., Amato, M. P., De Stefano, N., Enzinger, C., Geurts, J. J., Penner, I. K., Rovira, A., Sumowski, J. F., Valsasina, P., & Filippi, M. (2015). Clinical and imaging assessment of cognitive dysfunction in multiple sclerosis. In *The Lancet Neurology* (Vol. 14, Issue 3). https://doi.org/10.1016/S1474-4422(14)70250-9

Rocca, M. A., Sormani, M. P., Rovaris, M., Caputo, D., Ghezzi, A., Montanari, E., Bertolotto, A., Laroni, A., Bergamaschi, R., Martinelli, V., Comi, G., & Filippi, M. (2017). Long-term disability progression in primary progressive multiple sclerosis: A 15-year study. *Brain*, *140*(11). https://doi.org/10.1093/brain/awx250

Setiawan, E., Wilson, A. A., Mizrahi, R., Rusjan, P. M., Miler, L., Rajkowska, G., Suridjan, I., Kennedy, J. L., Rekkas, P. V., Houle, S., & Meyer, J. H. (2015). Role of translocator protein density, a marker of neuroinflammation, in the brain during major depressive episodes. *JAMA Psychiatry*, *72*(3). https://doi.org/10.1001/jamapsychiatry.2014.2427

Sheng, H., Zhao, B., & Ge, Y. (2019). Blood perfusion and cellular microstructural changes associated with iron deposition in multiple sclerosis lesions. *Frontiers in Neurology*, *10*(JUL). https://doi.org/10.3389/fneur.2019.00747

Sisco, N. J., Borazanci, A., Dortch, R., & Stokes, A. M. (2021). Investigating the relationship between multi-scale perfusion and white matter microstructural integrity in patients with relapsing-remitting MS. *Multiple Sclerosis Journal - Experimental, Translational and Clinical*, *7*(3). https://doi.org/10.1177/20552173211037002

Sokoloff, L., Reivich, M., Kennedy, C., Rosiers, M. H. D., Patlak, C. S., Pettigrew, K. D., Sakurada, O., & Shinohara, M. (1977). THE [14C]DEOXYGLUCOSE METHOD FOR THE MEASUREMENT OF LOCAL CEREBRAL GLUCOSE UTILIZATION: THEORY, PROCEDURE, AND NORMAL VALUES IN THE CONSCIOUS AND ANESTHETIZED ALBINO RAT. *Journal of Neurochemistry*, *28*(5). https://doi.org/10.1111/j.1471-4159.1977.tb10649.x

Sormani, M. P., Rovaris, M., Comi, G., & Filippi, M. (2009). A reassessment of the plateauing relationship between T2 lesion load and disability in MS. *Neurology*, *73*(19). https://doi.org/10.1212/WNL.0b013e3181c06679

Sowa, P., Bjørnerud, A., Nygaard, G. O., Damangir, S., Spulber, G., Celius, E. G., Due-Tønnessen, P., Harbo, H. F., & Beyer, M. K. (2015). Reduced perfusion in white matter lesions in multiple sclerosis. *European Journal of Radiology*, *84*(12). https://doi.org/10.1016/j.ejrad.2015.09.007

Strijbis, E. M. M., Kooi, E. J., van der Valk, P., & Geurts, J. J. G. (2017). Cortical remyelination is heterogeneous in multiple sclerosis. *Journal of Neuropathology and Experimental Neurology*, *76*(5). https://doi.org/10.1093/jnen/nlx023

Tateo, F., Grassivaro, F., Ermani, M., Puthenparampil, M., & Gallo, P. (2019). PM2.5 levels strongly associate with multiple sclerosis prevalence in the Province of Padua, Veneto Region, North-East Italy. *Multiple Sclerosis Journal*, *25*(13). https://doi.org/10.1177/1352458518803273

Thompson, A. J., Banwell, B. L., Barkhof, F., Carroll, W. M., Coetzee, T., Comi, G., Correale, J., Fazekas, F., Filippi, M., Freedman, M. S., Fujihara, K., Galetta, S. L., Hartung, H. P., Kappos, L., Lublin, F. D., Marrie, R. A., Miller, A. E., Miller, D. H., Montalban, X., … Cohen, J. A. (2018). Diagnosis of multiple sclerosis: 2017 revisions of the McDonald criteria. In *The Lancet Neurology* (Vol. 17, Issue 2). https://doi.org/10.1016/S1474-4422(17)30470-2

Tonietto, M., Rizzo, G., Veronese, M., Borgan, F., Bloomfield, P. S., Howes, O., & Bertoldo, A. (2019). A Unified Framework for Plasma Data Modeling in Dynamic Positron Emission Tomography Studies. *IEEE Transactions on Biomedical Engineering*, *66*(5). https://doi.org/10.1109/TBME.2018.2874308

Tonietto, M., Rizzo, G., Veronese, M., Fujita, M., Zoghbi, S. S., Zanotti-Fregonara, P., & Bertoldo, A. (2016). Plasma radiometabolite correction in dynamic PET studies: Insights on the available modeling approaches. In *Journal of Cerebral Blood Flow and Metabolism* (Vol. 36, Issue 2). https://doi.org/10.1177/0271678X15610585

Trapp, B. D., & Stys, P. K. (2009). Virtual hypoxia and chronic necrosis of demyelinated axons in multiple sclerosis. In *The Lancet Neurology* (Vol. 8, Issue 3). https://doi.org/10.1016/S1474-4422(09)70043-2

Trapp, B. D., Vignos, M., Dudman, J., Chang, A., Fisher, E., Staugaitis, S. M., Battapady, H., Mork, S., Ontaneda, D., Jones, S. E., Fox, R. J., Chen, J., Nakamura, K., & Rudick, R. A. (2018). Cortical neuronal densities and cerebral white matter demyelination in multiple sclerosis: a retrospective study. *The Lancet Neurology*, *17*(10). https://doi.org/10.1016/S1474-4422(18)30245-X

Trebossen, R., Bendriem, B., Ribeiro, M. J., Sarazin, M., Strul, D., Dupont, S., Semah, F., & Remy, P. (1999). Quantifying cerebral PET with FDG using dynamic internal carotid arteries imaging. *IEEE Nuclear Science Symposium and Medical Imaging Conference*, *3*. https://doi.org/10.1109/nssmic.1998.773875

Trojano, M., Tintore, M., Montalban, X., Hillert, J., Kalincik, T., Iaffaldano, P., Spelman, T., Sormani, M. P., & Butzkueven, H. (2017). Treatment decisions in multiple sclerosis-insights from real-world observational studies. In *Nature Reviews Neurology* (Vol. 13, Issue 2). https://doi.org/10.1038/nrneurol.2016.188

Turkheimer, F. E., Rizzo, G., Bloomfield, P. S., Howes, O., Zanotti-Fregonara, P., Bertoldo, A., & Veronese, M. (2015). The methodology of TSPO imaging with positron emission tomography. In *Biochemical Society Transactions* (Vol. 43). https://doi.org/10.1042/BST20150058

Veenman, L., & Gavish, M. (2006). The peripheral-type benzodiazepine receptor and the cardiovascular system. Implications for drug development. In *Pharmacology and Therapeutics* (Vol. 110, Issue 3). https://doi.org/10.1016/j.pharmthera.2005.09.007

Veenman, L., Leschiner, S., Spanier, I., Weisinger, G., Weizman, A., & Gavish, M. (2002). PK 11195 attenuates kainic acid-induced seizures and alterations in peripheral-type benzodiazepine receptor (PBR) protein components in the rat brain. *Journal of Neurochemistry*, *80*(5). https://doi.org/10.1046/j.0022-3042.2002.00769.x

Venneti, S., Wang, G., Nguyen, J., & Wiley, C. A. (2008). The positron emission tomography ligand DAA1106 binds with high affinity to activated microglia in human neurological disorders. *Journal of Neuropathology and Experimental Neurology*, *67*(10). https://doi.org/10.1097/NEN.0b013e318188b204

Vercellino, M., Masera, S., Lorenzatti, M., Condello, C., Merola, A., Mattioda, A., Tribolo, A., Capello, E., Mancardi, G. L., Mutani, R., Giordana, M. T., & Cavalla, P. (2009). Demyelination, inflammation, and neurodegeneration in multiple sclerosis deep gray matter. *Journal of Neuropathology and Experimental Neurology*, *68*(5). https://doi.org/10.1097/NEN.0b013e3181a19a5a

Vignal, N., Cisternino, S., Rizzo-Padoin, N., San, C., Hontonnou, F., Gelé, T., Declèves, X., Laure, S. M., & Hosten, B. T. (2018). [18F]FEPPA a TSPO radioligand: Optimized radiosynthesis and evaluation as a PET radiotracer for brain inflammation in a peripheral LPS-injected mouse model. *Molecules*, *23*(6). https://doi.org/10.3390/molecules23061375

Walton, C., King, R., Rechtman, L., Kaye, W., Leray, E., Marrie, R. A., Robertson, N., La Rocca, N., Uitdehaag, B., van der Mei, I., Wallin, M., Helme, A., Angood Napier, C., Rijke, N., & Baneke, P. (2020). Rising prevalence of multiple sclerosis worldwide: Insights from the Atlas of MS, third edition. *Multiple Sclerosis Journal*, *26*(14). https://doi.org/10.1177/1352458520970841

Werry, E. L., Bright, F. M., Piguet, O., Ittner, L. M., Halliday, G. M., Hodges, J. R., Kiernan, M. C., Loy, C. T., Kril, J. J., & Kassiou, M. (2019). Recent developments in TSPO PET imaging as a biomarker of neuroinflammation in neurodegenerative disorders. In *International Journal of Molecular Sciences* (Vol. 20, Issue 13). https://doi.org/10.3390/ijms20133161

Wimberley, C., Lavisse, S., Hillmer, A., Hinz, R., Turkheimer, F., & Zanotti-Fregonara, P. (2021). Kinetic modeling and parameter estimation of TSPO PET imaging in the human brain. In *European Journal of Nuclear Medicine and Molecular Imaging* (Vol. 49, Issue 1). https://doi.org/10.1007/s00259-021-05248-9

Wuerfel, J., Bellmann-Strobl, J., Brunecker, P., Aktas, O., McFarland, H., Villringer, A., & Zipp, F. (2004). Changes in cerebral perfusion precede plaque formation in multiple sclerosis: A longitudinal perfusion MRI study. *Brain*, *127*(1). https://doi.org/10.1093/brain/awh007

Yates, R. L., Esiri, M. M., Palace, J., Jacobs, B., Perera, R., & DeLuca, G. C. (2017). Fibrin(ogen) and neurodegeneration in the progressive multiple sclerosis cortex. *Annals of Neurology*, *82*(2). https://doi.org/10.1002/ana.24997

Zanotti-Fregonara, P., Chen, K., Liow, J. S., Fujita, M., & Innis, R. B. (2011). Image-derived input function for brain PET studies: Many challenges and few opportunities. In *Journal of Cerebral Blood Flow and Metabolism* (Vol. 31, Issue 10). https://doi.org/10.1038/jcbfm.2011.107

Zhang, L., Hu, K., Shao, T., Hou, L., Zhang, S., Ye, W., Josephson, L., Meyer, J. H., Zhang, M. R., Vasdev, N., Wang, J., Xu, H., Wang, L., & Liang, S. H. (2021). Recent developments on PET radiotracers for TSPO and their applications in neuroimaging. In *Acta Pharmaceutica Sinica B* (Vol. 11, Issue 2). https://doi.org/10.1016/j.apsb.2020.08.006